AD-A053 077 CORNELL UNIV ITHACA N Y LAB OF PLASMA STUDIES F/G 7/4
STUDIES OF LASER INDUCED PHOTOCHEMICAL KINETICS.(U)
DEC 77 R A MCFARLANE AFOSR-75-2781
UNCLASSIFIED AFOSR-TR-78-0568 NL

| OF |
AD A053077

END
DATE FILMED
5 -78
DDC

STUDIES OF LASER INDUCED PHOTOCHEMICAL KINETICS

Grant 75-2781

Air Force Office of Scientific Research

Final Report

1 September 1974-31 August 1977

Approved for public release;
distribution unlimited.

Laboratory of Plasma Studies
Cornell University
Ithaca, New York 14853

SECURITY CLASSIFICATION OF THIS PAGE (When Data Entered)

REPORT DOCUMENTATION PAGE

READ INSTRUCTIONS BEFORE COMPLETING FORM

1. REPORT NUMBER: AFOSR-TR-78-0568	2. GOVT ACCESSION NO.
3. RECIPIENT'S CATALOG NUMBER	
4. TITLE (and Subtitle): STUDIES OF LASER INDUCED PHOTOCHEMICAL KINETICS.	5. TYPE OF REPORT & PERIOD COVERED: FINAL rept. 1 Sep 74 — 31 Aug 77
	6. PERFORMING ORG. REPORT NUMBER
7. AUTHOR(s): R. A. McFarlane	8. CONTRACT OR GRANT NUMBER(s): AFOSR-75-2781
9. PERFORMING ORGANIZATION NAME AND ADDRESS: Cornell University, Laboratory of Plasma Studies, Ithaca, NY 14853	10. PROGRAM ELEMENT, PROJECT, TASK AREA & WORK UNIT NUMBERS: 61102F, 2303/B1
11. CONTROLLING OFFICE NAME AND ADDRESS: Air Force Office of Scientific Research/NC, Bolling AFB DC 20332	12. REPORT DATE: Dec 77
	13. NUMBER OF PAGES: 83
14. MONITORING AGENCY NAME & ADDRESS (if different from Controlling Office): 68 p.	15. SECURITY CLASS. (of this report): UNCLASSIFIED
	15a. DECLASSIFICATION/DOWNGRADING SCHEDULE

16. DISTRIBUTION STATEMENT (of this Report)

Approved for public release; distribution unlimited.

ACCESSION for	
NTIS	White Section [X]
DDC	Buff Section [ ]
UNANNOUNCED	[ ]
JUSTIFICATION	
BY	
DISTRIBUTION/AVAILABILITY CODES	
Dist.	AVAIL. and/or SPECIAL
A	

17. DISTRIBUTION STATEMENT (of the abstract entered in Block 20, if different from Report)

18. SUPPLEMENTARY NOTES

19. KEY WORDS (Continue on reverse side if necessary and identify by block number)

Iodine Laser
Electronic State Quenching
Photochemical Kinetics
Collisional Release

20. ABSTRACT (Continue on reverse side if necessary and identify by block number)

Second order quenching rate constants are reported for the quenching of excited iodine atoms ($5p^5\ ^2P_{1/2}$) by selected molecules. These include I_2, O_2, H_2O, D_2O, H_2O_2, CO_2, N_2, H_2, HD, D_2. Temperature dependence studies were made over the range 295°K-600°K. Complex photodecomposition kinetics were observed for I_2 and modelled.

DD FORM 1 JAN 73 1473 EDITION OF 1 NOV 65 IS OBSOLETE

UNCLASSIFIED

SECURITY CLASSIFICATION OF THIS PAGE (When Data Entered)

403200

Introduction

The research carried out under this grant was in support of work being done at the Air Force Weapons Laboratory to develop a continuously operating laser system based on the transition in atomic iodine

$$I(5p^5\ ^2P_{1/2}) \rightarrow I(5p^5\ ^2P_{3/2}) + h\nu(1.315\ \mu) \qquad (1)$$

The excitation mechansim is based on the near resonant energy exchange between $O_2(^1\Delta)$ molecules and ground state iodine atoms

$$I + O_2(^1\Delta) \rightarrow I^* + O_2(^3\Sigma) \qquad (2)$$

Molecular oxygen in the $^1\Delta$ electronic state is produced chemically or electrically and iodine is introduced into a continuously flowing stream of excited oxygen, ultimately leading to the production of a population inversion on the 1.315 μ transition.

A model of the chemical and lasing kinetics of this system has been developed at AFWL by Franklin and can be used to determine optimum operating parameters and scaling information. Included in this model are processes

$$I^* + M \rightarrow I + M \qquad (3)$$

which de-excite the upper state laser level as a result of collisions with molecules M. It is important therefore, since (3) is in direct

competition with stimulated emission for the available energy, that accurate information be available on the second order quenching rate constants for the molecules M present in the system.

During the early stages of this program a substantial amount of instrumentation was developed to permit the observation of very high speed photodecomposition kinetics following laser photolyses of molecular iodine and related compounds. This has been discussed in detail in a Ph.D. thesis by D. H. Burde which formed the bulk of the report on this Grant for the period September 1975-August 1976. The apparatus was used to determine a number of the quenching rate constants required above and more recently to examine their behaviour as a function of temperature. These temperature studies represent the new work carried out during the past grant period and have been described in a paper to be submitted to the Journal of Chemical Physics. This paper is included as a part of this present report.

Results and Publications

a) Quenching Rates

The quenching of $I(^2P_{1/2})$ atoms by various species has received some previous attention in the literature. Our initial studies with $M = I_2$ indicated a second order quenching rate constant almost an order of magnitude larger than the previously accepted value and indicated measurements should also be carried out for other potential quenchers in the iodine atom laser system in order to have reliable data for model kinetic computations.

Second order quenching rate constants at 295° K for deactivation of I* by I_2, O_2, H_2O, D_2O, H_2O_2, CO_2, N_2, H_2, HD and D_2 have been determined. For I_2, O_2, H_2, HD and D_2 measurements have been carried out on the temperature dependence of the rate constants between 295° K and 600° K.

Publication of this work has appeared as follows:

D. H. Burde, R. A. McFarlane and J. R. Wiesenfeld, Chem. Phys. Lett. 32, 296 (1975).

D. H. Burde and R. A. McFarlane, J. Chem. Phys. 64, 1850 (1976).

D. H. Burde and R. A. McFarlane-studies on temperature dependence-submitted to J. Chem. Phys. and included in this report.

D. H. Burde, Ph.D. Thesis, Cornell University, September 1976.

b) Collisional Release and Complex Photodecomposition Kinetics

By studying the pressure dependence of the appearance rate of excited iodine atoms following short pulse laser photolysis of molecular iodine below the dissociation limit, it has been possible to demonstrate that excited atom production is consistent with the process

$$I_2(B\ ^3\Pi_{o_u^+}) + M \rightarrow I^*\ (5\ ^2P_{1/2}) + I(5\ ^2P_{3/2}) + M$$

where M = I_2 or N_2. A kinetic model has been set up which shows that the appearance rate of I* from this process should be equal to the decay rate of the I_2 B state fluorescence. Careful computer fitting of the U.V. absorption data which represents I* population does indeed

indicate a production component of the correct form.

The laser induced decomposition of I_2 is however more complex. A second pathway for the production of excited iodine atoms was found having a different rate from the "Collisional Release" mechanism above. The process also proceeds as a result of collisions but involves an electronic state of I_2 other than the B state. The identity of this state has yet to be unambiguously established.

Efforts to determine that a two photon absorption process is responsible leading to the excitation of an electronic state of I_2 above the B state have been inconclusive and more measurements are required. The electronic state is clearly a bound state, possibly the $^3\Sigma_u^-$ state correlating with $^3P_2$ and ^1S ionic atom states. The data obtained provide information on the quenching rate of this state by both I_2 and N_2 molecules.

The significance of the observations is however that two photon excitation mechanisms may indeed be adequately strong to provide molecular excited state population of adequate species concentration to be of value in kinetics observations. Previous two photon studies have largely been directed at obtaining only spectroscopic information.

This work has been published as:

D. H. Burde and R. A. McFarlane, Chem. Phys. 16, 295 (1976).

c) Lineshape Effects

The use of atomic absorption spectroscopy under conditions similar to those in the present experiments can lead to the necessity of modifying the simple Beer-Lambert law of absorption by an empirical constant γ which must be determined by measurement over the range of experimental parameters. A series of computations were made designed to explore the validity of such a modification and to determine, if possible, conditions under which it can be employed. It was found in particular that for the measurements of iodine atom kinetics reported here only a small modification of the Beer-Lambert law is required and indeed our measured quenching rates (γ corrected) have been found to be in excellent agreement with subsequent observations made using fluorescence techniques.

This work has been puslished as:

C. C. Davis and R. A. McFarlane, J.Q.S.R.T. 18, 151 (1977).

Abstract of Objectives and Accomplishments

A new experimental technique has been developed to study gas phase kinetics on a timescale more than two orders of magnitude faster than previously possible. The kinetics of the collisional production and deactivation of electronically excited iodine atoms, $I^*(^2P_{1/2})$, were studied by selectively photolyzing molecular I_2 with a short pulse (10 nsec) tunable dye laser. The excited atom population as a function of time following each laser pulse was detected by photoelectrically monitoring the absorption of atomic iodine resonance radiation at 206.2 nm. In this way, kinetic processes on a tens-of-nanosecond timescale were observable.

The primary goal of the project was to obtain the collisional quenching rates of $I^*(^2P_{1/2})$ by several collision partners of interest in pulsed and CW iodine laser systems. The nonradiative decay by collisional quenching is an important loss mechanism in these lasers and accurate quenching rates are required for computer modelling and efficient laser design. A systematic study of the quenching rate of I* as a function of added gas pressure was undertaken. By using a relatively low energy photolysis pulse and employing signal averaging to improve signal-to-noise ratios, many problems which complicated earlier high-energy flash photolysis studies were eliminated. High precision pressure measuring equipment and computer analysis of the digitized waveforms permitted accurate determination of the second order quenching rate constants at 295° K for deactivation of I* by I_2, O_2, H_2O, D_2O, H_2O_2, CO_2, N_2, H_2, HD, and D_2. Very significant

differences in quenching efficiency were observed in isotopically substituted species and a very high quenching efficiency was found for I_2 and also for O_2, for which a near resonance E → E energy transfer occurs with I*. To further probe the physical processes causing the quenching, the temperature dependence of the quenching rates for I_2, O_2, H_2, HD, and D_2 were determined. Results of the temperature dependence studies supported the importance of resonant E → V energy transfer for deactivation by H_2, HD, and D_2. The quenching rate was found to increase with temperature for both I_2 and O_2, with small activation energies for each.

The second major area of work involved the study of the collisional production of excited atoms (I*) from bound electronically excited states of I_2. Significant production of I* was found for excitation as much as 4.5 kT below the dissociation limit of the I_2(B) state. Using the high speed photolysis system, the concentration of I* was seen to continue to rise for several hundred nanoseconds after the laser pulse. By studying the detailed behavior of the rising portion of the signal as a function of pressure, the collisional production of I* atoms from bound states of I_2 was confirmed and a kinetic model for this "collisional release" process was developed. In addition, evidence of two photon absorption to a higher lying bound electronic state was uncovered and collisional decomposition from this state was also measured.

The high speed photolysis system developed in the course of this work is extremely versatile and attractive for a variety of gas phase kinetic studies. It provides selective excitation and selective observation as well as excellent sensitivity and speed.

Publications

"Studies of the Deactivation of Electronically Excited Iodine Atoms," D. H. Burde, R. A. McFarlane, and J. R. Wiesenfeld, presented at the Fourth Conference on Chemical and Molecular Lasers, October 21-23, 1974, St. Louis, Missouri.

"Quantum Efficiencies for the Production of Electronically Excited Iodine Atoms $I(5p^5\ ^2P_{1/2})$ Following Laser Photolysis of I_2 Near 5000Å," D. H. Burde, R. A. McFarlane, J. R. Wiesenfeld, Phys. Rev. A10, 1917 (1974).

"Collisional Quenching of Excited Iodine Atoms $I(5p^5\ ^2P_{1/2})$ by I_2," D. H. Burde, R. A. McFarlane, and J. R. Wiesenfeld, Chem. Phys. Lett. 32, 296 (1975).

"Collisional Quenching of Excited Iodine Atoms," D. H. Burde, C. C. Davis, and R. A. McFarlane, presented at the Second Summer Colloquium on Electronic Transition Lasers, September 17-19, 1975, Woods Hole, Massachusetts.

"Collisional Quenching of Excited Iodine Atoms $I\ (5p^5\ ^2P_{1/2})$ by Selected Molecules," D. H. Burde and R. A. McFarlane, J. Chem. Phys. 64, 1850 (1976).

"Observation of Collisional Release and Complex Photodecomposition Kinetics of Molecular Iodine," D. H. Burde and R. A. McFarlane, presented at the Third Summer Colloquium on Electronic Transition Lasers, September 7-10, 1976, Snowmass Village, Colorado.

"Production of Electronically Excited Iodine Atoms $I(5p^5\ ^2P_{1/2})$ by Collisional Release in Molecular I_2," D. H. Burde and R. A. McFarlane, Chem. Phys. 16, 295 (1976).

"Lineshape Effects in Atomic Absorption Spectroscopy," C. C. Davis and R. A. McFarlane, J.Q.S.R.T. 18, 151 (1977).

"Temperature Dependence of the Collisional Deactivation of Excited Iodine Atoms $I(5p^5\ ^2P_{1/2})$," D. H. Burde and R. A. McFarlane, submitted to J. Chem. Phys.

Conference Papers Read

D. H. Burde, R. A. McFarlane and J. R. Wiesenfeld, "Studies of the Deactivation of Excited Iodine Atoms", presented at the Fourth Conference on Chemical and Molecular Lasers, St. Louis, Missouri, October 21-23, 1974.

R. A. McFarlane, "Review of Electron Collision Pumping of Electronic Transition Lasers", invited paper at Fifth Winter Colloquium on Quantum Electronics, Snowmass, Colorado, February 1-5, 1975.

D. H. Burde, C. C. Davis and R. A. McFarlane, "Collisional Quenching of Excited Iodine Atoms", presented at the Second Summer Colloquium on Electronic Transition Lasers, Woods Hole, Massachusetts, September 17-19, 1975.

D. H. Burde and R. A. McFarlane, "Observation of Collisional Release and Complex Photodecomposition Kinetics of Molecular Iodine", presented at the Third Summer Colloquium on Electron Transition Lasers, Snowmass, Colorado, September 7-10, 1976.

J. Quant. Spectrosc. Radiat. Transfer. Vol. 18, pp. 151–170. Pergamon Press 1977. Printed in Great Britain

LINESHAPE EFFECTS IN ATOMIC ABSORPTION SPECTROSCOPY

CHRISTOPHER C. DAVIS†‡ and ROSS A. MCFARLANE§
Cornell University, Ithaca, NY 14853, U.S.A.

(*Received* 13 *February* 1976)

Abstract—Deviations from Beer's Law caused by the relative lineshape functions of source and absorber in atomic absorption experiments are considered. The validity of using a modified form of the law incorporating a correction factor γ, which is particularly convenient in time-resolved atomic absorption experiments, to account for these deviations, has been critically examined for a wide range of source and absorber lineshapes using numerical evaluation of the transmission integrals involved. It is concluded that there is, in general, no theoretical justification for the use of such a γ factor, except in the case of large source linewidth/absorber linewidth ratios when the line broadening in the absorber involves a significant homogeneous (Lorentzian) contribution. The use of empirically determined γ factors, much different from unity to analyse experimental data, should be viewed with suspicion unless direct evidence is presented to show that under the experimental conditions γ happens to be constant or slowly varying.

INTRODUCTION

THE ABSORPTION coefficient at frequency ν of a spectral line with a normalized lineshape function $g(\nu)$ is[1]

$$\alpha(\nu) = (\lambda_0^2 A_{21} g_2/8\pi g_1)[N_1 - (g_1/g_2)N_2]g(\nu), \tag{1}$$

where the symbols have their usual significance. In a medium with such an absorbing line, the intensity of radiation transmitted a distance s through the medium, if saturation effects are negligible, satisfies Beer's law

$$I = I_0 \exp(-\alpha s), \tag{2}$$

where I_0 is the intensity of the radiation at $s = 0$. If $g(\nu)$ is determined predominantly by homogeneous broadening, it is given by the normalized Lorentzian lineshape function

$$g_L(\nu) = (2/\pi\Delta\nu_N)/\{1 + [2(\nu - \nu_0)/\Delta\nu_N]^2\}, \tag{3}$$

where ν_0 is the line centre frequency and $\Delta\nu_N$ is the full width at half maximum height (FWHM) of the line. When inhomogeneous broadening predominates, $g(\nu)$ is given by the normalized Gaussiah lineshape function

$$g_D(\nu) = (2/\Delta\nu_D)(\ln 2/\pi)^{1/2} \exp\{-[2(\nu - \nu_0)/\Delta\nu_D]^2 \ln 2\}, \tag{4}$$

where $\Delta\nu_D$ is the FWHM of the line. With both Lorentzian and Gaussian broadening, the lineshape function is given by the normalized Voigt profile[1,2]

$$g_v(\nu) = (2/\Delta\nu_D)(\ln 2/\pi)^{1/2} \frac{y}{\pi} \int_{-\infty}^{\infty} \frac{e^{-t^2}}{y^2 + (x - t)^2} dt, \tag{5}$$

where $y = \Delta\nu_N \ln 2)^{1/2}/\Delta\nu_D$ and $x = 2(\nu - \nu_0)(\ln 2)^{1/2}/\Delta\nu_D$; $\Delta\nu_N$ and $\Delta\nu_D$ are the FWHM of the Lorentzian and Gaussian contributions to the total lineshape.

The Voigt profile can be written in terms of the real part of the error function for complex argument $\mathcal{R}W(z)$[3] as

$$g_v(\nu) = (2/\Delta\nu_D)(\ln 2/\pi)^{1/2} \mathcal{R}W(z), \tag{6}$$

†Present address: Electrical Engineering Department, University of Maryland, College Park, MD 20742, U.S.A.
‡School of Applied and Engineering Physics and Materials Science Center.
§School of Electrical Engineering, Materials Science Center and Laboratory of Plasma Studies.

where $z = x + iy$. The function $W(z)$ has been tabulated;[3,4] it is related to the plasma dispersion function $Z(z)$ tabulated by FRIED and CONTE[5] by

$$W(z) = Z(z)/i\pi^{1/2}. \tag{7}$$

The absorption coefficient of a medium with a Voigt profile is then

$$\alpha(\nu) = \alpha_0 \mathcal{R} W(z), \tag{8}$$

where α_0 is the same as the absorption coefficient at the centre of a Gaussian line and is given by the expression

$$\alpha_0 = \frac{1}{4\pi}\left(\frac{\ln 2}{\pi}\right)^{1/2} \frac{\lambda_0^2 g_2 A_{21}}{g_1 \Delta\nu_D}[N_1 - (g_1/g_2)N_2]. \tag{9}$$

In most situations encountered in atomic absorption spectroscopy, $N_2 \ll N_1$ and we may write $N_1 = N$ and

$$\alpha_0 = k_0 N, \tag{10}$$

where

$$k_0 = \frac{1}{4\pi}\left(\frac{\ln 2}{\pi}\right)^{1/2} \lambda_0^2 \frac{g_2 A_{21}}{g_1 \Delta\nu_D}. \tag{11}$$

It is clear from eqns (8) and (9) that monochromatic absorption measurements at ν yield information about N_1 (provided $N_2 \ll N_1$) and A_{21}, provided the lineshape function of the absorber is known.

In practice, it is difficult to find an ideal monochromatic source. Tunable dye lasers can be used, but care must be taken to ensure that their emission frequencies are stable. In some cases, the laser may be operated on the transition used in absorption [as in determinations of ground state atomic iodine concentrations[6]]. In general, however, atomic absorption experiments, are performed with incoherent line sources involving the atoms studied in absorption.

If the total source intensity reaching the detection system, in the absence of absorbing material, is I_0, then the total detected emission in a small frequency range $d\nu$ at frequency ν is $I_0 g_s(\nu)\, d\nu$, where $g_s(\nu)$ is the normalized source lineshape function; $g_s(\nu)$ includes all the effects of line broadening and reabsorption within the source, as well as any convolution of the spontaneous emission lineshape function of the source with the frequency transmission function of optical elements between source and absorber.[17]

For a spatially uniform concentration of absorbing material of constant geometrical length, the observed intensity is

$$I = I_0 \int_{-\infty}^{\infty} g_s(\nu)\, e^{-\alpha(\nu)L}\, d\nu, \tag{12}$$

where $\alpha(\nu) = kNg(\nu)$ and $k = \lambda_0^2 A_{21} g_2/8\pi g_1$. Expanding the exponential in eqn (12), the transmission becomes

$$T = I/I_0 = 1 - aF + bF^2/2! - cF^3/3! + \cdots, \tag{13}$$

where $F = kNL\sigma$ and σ is the value of $g(\nu)$ at the line centre. The coefficients $a, b, c, \ldots$, are given by the expressions

$$a = \frac{1}{\sigma}\int_{-\infty}^{\infty} g_s(\nu)g(\nu)\, d\nu, \quad b = \frac{1}{\sigma^2}\int_{-\infty}^{\infty} g_s(\nu)[g(\nu)]^2\, d\nu, \quad c = \frac{1}{\sigma^3}\int_{-\infty}^{\infty} g_s(\nu)[g(\nu)]^3\, d\nu \ldots$$

For small absorptions ($F \ll 1$), eqn (13) gives

$$\ln (I/I_0) = -\frac{F}{\sigma}\int_{-\infty}^{\infty} g_s(\nu)g(\nu)\,\mathrm{d}\nu. \tag{14}$$

In this case, a graph of $\ln (I_0/I)$ vs F is linear and Beer's law holds. However, when the total absorption is not very small, eqn (13) shows that graphs of $\ln (I_0/I)$ vs F are no longer linear. The resultant "curves of growth" have received considerable attention.

Determination of the transmission of an absorber from the series expansion given in eqn (13) is not practicable for $F > 1$ as the series converges slowly and it is better to evaluate the integral in eqn (12) directly. Some results of this type have been given by PRUGGER[9] for sources and absorbers having Lorentzian or Gaussian lineshapes. If the source and absorber lineshapes are known, the coefficients a, b, c... can be determined. For small values of F, a function containing the first few terms of eqn (13) can then be fitted to an experimentally determined curve of T vs relative absorber concentration to determine F. This method has been used by MORSE and KAUFMAN,[10] PARKES, KEYSER and KAUFMAN[11] and KAUFMAN and PARKES[12] by assuming both source and absorber to have Doppler profiles, while BRAUN and CARRINGTON[13] have considered the effect which self-reversal of the source has on the transmission of a given Doppler-broadened absorber. Alternatively, a "best fit" to an experimentally determined curve of transmission vs relative absorber concentration can be used to find empirical values for a, b, c..., and hence F, without specific knowledge of source and absorber lineshapes,[14,15] although a unique "best fit" may be difficult to find. If this occurs, improved results can be obtained by comparing observations made with different sources[15] (which should have different lineshape functions). These various techniques for taking into account source and absorber lineshape effects in atomic absorption measurements have been compared by BEMAND and CLYNE[16] for a few combinations of source and absorber lineshapes. Further distortion of transmission vs relative absorber concentration curves occurs if the source and absorber lines are closely spaced multiplets or have resolved hyperfine structure. However, this problem can generally be dealt with by one of the listed methods of analysis.[10–12,14–16]

An empirical, modified version of Beer's Law has been proposed[18] which accommodates the effect of source and absorber lineshapes and is particularly convenient to use in time-resolved atomic absorption measurements. This modified form of Beer's Law, which should be compared with eqn (13), can be written as

$$T = I/I_0 = \mathrm{e}^{-(F)^{\gamma}}, \tag{15}$$

where γ has been assumed independent of absorber concentration over the range of absorber concentrations used in very many time-resolved atomic absorption experiments.[18–27,31] In such experiments, if the transient absorbing species decays exponentially, then $F = F_0\,\mathrm{e}^{-t/\tau}$. Then, if use of eqn (15) can be justified,

$$\ln \ln (1/T) = \gamma t/\tau + \gamma \ln F_0, \tag{16}$$

which allows determination of τ from a graph of $\ln \ln (1/T)$ vs t if γ is known.

As is discussed briefly by BEMAND and CLYNE,[16] it is difficult to justify the use of such a γ factor theoretically, as is evident by comparing eqn (13) and the series expansion of eqn (15), viz.

$$T = I/I_0 = 1 - F^{\gamma} + \frac{F^2\gamma}{2!} - \frac{F^3\gamma}{3!} + \cdots. \tag{17}$$

Only as $\gamma \to 1$ and a, b, $c \to 1$ do eqns (13) and (17) become equivalent. However, the use of such a γ factor has been demonstrated to be empirically correct in several experiments from the relatively good linearity of $\ln \ln (1/T)$ vs $\ln F$ plots.[18,21–24,31]

It is our purpose in this article to consider carefully when the use of such an empirical γ factor may be justified. To this end, we have numerically evaluated the integral in eqn (12) for a

large number of source/absorber lineshape combinations over a wide range of absorption coefficients. To test the validity of eqn (15), we have computed curves of $\ln \ln (I_0/I)$ vs $\ln F$ for each source/absorber lineshape combination. By numerically differentiating these curves we have thus determined an effective γ as a function of absorption and have concluded that, in general, γ is not independent of absorber concentration. We will deal, in turn, with the results for each of the combinations we have studied.

(i) *Doppler-broadened source and absorber*

In this case, from eqns (4) and (12) and writing $\Delta\nu_s$, $\Delta\nu_a$ for the Doppler widths (FWHM) of the source and absorber lineshapes, respectively,

$$I/I_0 = \int_{-\infty}^{\infty} \frac{2}{\Delta\nu_s}\left(\frac{\ln 2}{\pi}\right)^{1/2} \exp\{-[2(\nu-\nu_0)/\Delta\nu_s]^2 \ln 2\} \times \exp[-F \exp\{-[2(\nu-\nu_0)\Delta\nu_a]^2 \ln 2\}]\, d\nu. \tag{18}$$

Expanding the second exponential, this gives

$$I/I_0 = 1 - F[(\Delta\nu_s/\Delta\nu_a)^2 + 1]^{1/2} + F^2/2![2(\Delta\nu_s/\Delta\nu_a)^2 + 1]^{1/2} - F^3/3![3(\Delta\nu_s/\Lambda\nu_a)^2 + 1]^{1/2} + \cdots, \tag{19}$$

where, for a Doppler-broadened absorber,

$$F = kNL\sigma = \frac{1}{4\pi}\left(\frac{\ln 2}{\pi}\right)^{1/2} \frac{\lambda_0^2 A_{21}}{\Delta\nu_a}\frac{g_2}{g_1} NL. \tag{20}$$

However, we have evaluated the integral in eqn (18) numerically to determine the dependence of T on absorber concentration. The integral was rewritten in the form

$$I/I_0 = 2\int_0^{\infty} 2(\ln 2/\pi)^{1/2} \exp[-4(\Delta\nu)^2 \ln 2] \exp\{-F \exp[-4(w\Delta\nu)^2 \ln 2]\}\, d\Delta\nu, \tag{21}$$

where $w = \Delta\nu_s/\Delta\nu_a$ and $(\nu - \nu_0)/\Delta\nu_s = \Delta\nu$; computation was truncated 10 linewidths from the line centre.[32]

To determine curves of growth, the integral in eqn (21) was evaluated at uniformly spaced values of $\ln F$ between $\ln F = -4$ and $\ln F = 4$ for values of the source/absorber linewidth ratio between 0.1 and 10. Some typical curves of growth obtained in this way are shown in Fig. 1. However, of more interest are the curves shown in Fig. 2 and tabulated in Table 1, which illustrate the dependence of the γ factor on observed absorption.

It is clear that, when γ deviates significantly from unity, it is not independent of absorption,

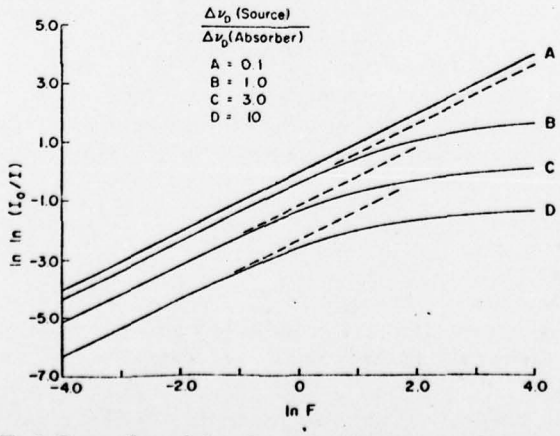

Fig. 1. Curves of growth for a Doppler-broadened source and absorber.

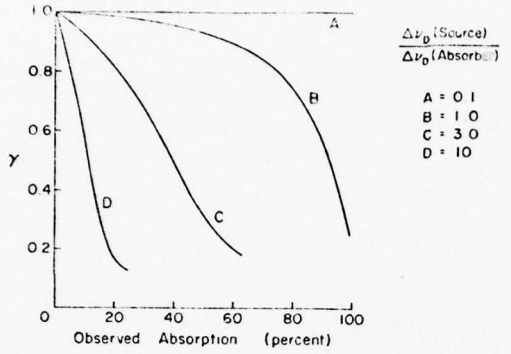

Fig. 2. γ factor variation with observed absorption for a Doppler-broadened source and absorber.

Table 1. γ factor variation with observed transmittance for a Doppler-broadened source and absorber

$\frac{\Delta\nu_D \text{ (Source)}}{\Delta\nu_D \text{ (Absorber)}}$	0.1		1.0		3.0		10.0	
lnF	T	γ	T	γ	T	γ	T	γ
-3.2	0.9603	1.000	0.9717	0.997	0.9873	0.991	0.9960	0.986
-2.4	0.9137	1.000	0.9382	0.994	0.9722	0.979	0.9913	0.970
-1.6	0.8180	1.000	0.8683	0.987	0.9406	0.954	0.9813	0.934
-0.8	0.6395	1.000	0.7337	0.970	0.8785	0.898	0.9616	0.853
0.0	0.3697	1.000	0.5139	0.925	0.7728	0.778	0.9279	0.712
0.4	0.2264	1.000	0.3829	0.879	0.7055	0.682	0.9062	0.606
0.8	0.1092	1.000	0.2577	0.803	0.6356	0.565	0.8833	0.488
1.2	0.0368	1.000	0.1773	0.686	0.5706	0.442	0.8615	0.375
1.4	0.0177	1.000	0.1198	0.615	0.5417	0.388	0.8516	0.327
1.6	0.0072	1.000	0.0907	0.542	0.5156	0.341	0.8424	0.287
1.8	0.0024	1.000	0.0689	0.475	0.4920	0.304	0.8339	0.255
2.0	0.0006	1.000	0.0528	0.419	0.4706	0.274	0.8260	0.230
2.2	0.0001	1.000	0.0408	0.375	0.4510	0.253	0.8186	0.210
2.4	0.0000	1.000	0.0318	0.340	0.4329	0.232	0.8116	0.194
2.6	0.0000	1.000	0.0250	0.313	0.4161	0.216	0.8050	0.180
2.8	0.0000	0.999	0.0197	0.290	0.4003	0.203	0.7986	0.169
3.0	0.0000	0.999	0.0155	0.271	0.3854	0.191	0.7924	0.159
3.2	0.0000	0.999	0.0123	0.255	0.3714	0.181	0.7865	0.150

invalidating the use of the modified Beer's law when a Doppler-broadened source and absorber are used. Only for small values of w, (e.g. the 0.1 curve in Fig. 2) does the absorption follow Beer's law up to large absorptions with a value of γ close to unity.

(ii) *Doppler-broadened source and Lorentzian-broadened absorber*

The transmission integral evaluated in this case was

$$I/I_0 = 2\int_{-\infty}^{\infty} 2(\ln 2/\pi)^{1/2} \exp[-4(\Delta\nu)^2 \ln 2] \exp\{-F[1+4(w\Delta\nu)^2]^{-1}\}\Delta\nu, \qquad (22)$$

where $w = \Delta\nu_D$ (source)/$\Delta\nu_N$ (absorber). Some typical results from these computations are

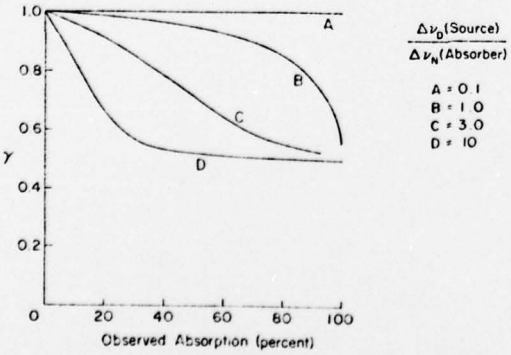

Fig. 3. γ factor variation with observed absorption for a Doppler-broadened source and Lorentzian-broadened absorber.

shown in Fig. 3 and Table 2. In this case, for large values of the source/absorber linewidth ratio, γ changes more slowly with absorption than with a Doppler-broadened absorber and becomes approximately constant for large linewidth ratios and absorptions.

(iii) *Lorentzian-broadened source and absorber*

The transmission integral to be evaluated in this case is

$$I/I_0 = 2\int_{-\infty}^{\infty} \frac{2}{\pi}[1+4(\Delta\nu)^2]^{-1} \exp\{-F[1+4(w\Delta\nu)^2]^{-1}\}\, d\Delta\nu, \tag{23}$$

where $w = \Delta\nu_N$ (source)/$\Delta\nu_N$ (absorber). This integral can be evaluated in series as

$$I/I_0 = 1 - \frac{F}{1+w} + \frac{F^2}{2!}\frac{(2+w)}{2(1+w)^2} - \frac{F^3}{3!}\frac{(8+9w+3w^2)}{8(1+w)^3} + \frac{F^4}{4!}\frac{(16+29w+20w^2+5w^3)}{(1+w)^4} - \frac{F^5}{5!}\frac{(128+325w+325w^2+175w^3+35w^4)}{128(1+w)^5} + \cdots \tag{24}$$

However, convergence of this series is poor for $F > 1$ making direct numerical evaluation of eqn (23) desirable. Because a source with a Lorentzian lineshape has considerable energy in its wings, the integral was truncated at 1000 linewidths from the line centre. Some typical results from these computations are shown in Fig. 4 and Table 3. The trend towards a more slowly changing γ with absorption for large values of w is again evident. For large values of w, so much of the emission intensity of the source lies outside the region where useful absorption occurs, that large absorptions are not observed for the maximum values of F used in our computations.

(iv) *Lorentzian-broadened source and Doppler-broadened absorber*

The transmission integral evaluated in this case was

$$I/I_0 = 2\int_{0}^{\infty} \frac{2}{\pi}[1+4(\Delta\nu)^2]^{-1} \exp\{-F\exp[-4(w\Delta\nu)^2 \ln 2]\}\, d\Delta\nu, \tag{25}$$

where $w = \Delta\nu_N$ (source)/$\Delta\nu_D$ (absorber). Typical results from these computations are shown in

Table 2. γ factor variation with observed transmittance for a Doppler-broadened source and Lorentzian-broadened absorber

$\Delta\nu_D$ (Source) / $\Delta\nu_D$ (Absorber)	0.1		1.0		3.0		10.0	
lnF	T	γ	T	γ	T	γ	T	γ
-3.2	0.9603	1.000	0.9717	0.998	0.9851	0.994	0.9946	0.991
-2.4	0.9139	1.000	0.9382	0.996	0.9675	0.987	0.9881	0.980
-1.6	0.8183	1.000	0.8683	0.990	0.9300	0.971	0.9742	0.956
-0.8	0.6401	1.000	0.7328	0.978	0.8552	0.936	0.9461	0.906
0.0	0.3705	1.000	0.5093	0.948	0.7228	0.863	0.8944	0.814
0.4	0.2274	1.000	0.3741	0.919	0.6338	0.807	0.8576	0.750
0.8	0.1097	1.000	0.2431	0.874	0.5349	0.738	0.8139	0.681
1.2	0.0470	1.000	0.1462	0.808	0.4342	0.666	0.7644	0.618
1.4	0.0179	1.000	0.0960	0.768	0.3855	0.634	0.7379	0.593
1.6	0.0073	1.000	0.0651	0.728	0.3389	0.607	0.7101	0.573
1.8	0.0025	1.000	0.0424	0.687	0.2947	0.585	0.6812	0.557
2.0	0.0007	1.000	0.0266	0.653	0.2532	0.569	0.6511	0.545
2.2	0.0001	0.999	0.0161	0.625	0.2146	0.556	0.6197	0.536
2.4	0.0000	0.999	0.0093	0.604	0.1796	0.547	0.5870	0.530
2.6	0.0000	0.999	0.0051	0.587	0.1468	0.539	0.5533	0.524
2.8	0.0000	0.999	0.0026	0.575	0.1180	0.533	0.5181	0.520
3.0	0.0000	0.998	0.0013	0.565	0.0928	0.528	0.4820	0.517
3.2	0.0000	0.998	0.0006	0.556	0.0712	0.524	0.4452	0.514
3.6							0.3703	0.510
4.0							0.2959	0.507
4.4							0.2251	0.505
4.8							0.1614	0.504
5.2							0.1073	0.503
5.6							0.0653	0.502
6.0							0.0358	0.502
6.4							0.0170	0.501
6.8							0.0069	0.501
7.2							0.0023	0.501

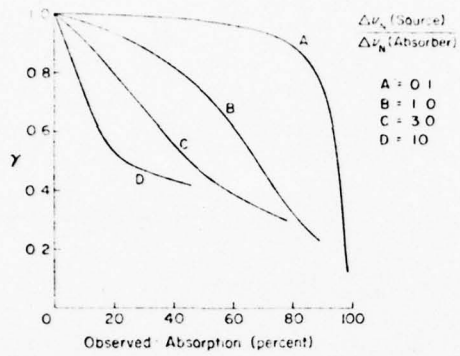

Fig. 4. γ factor variation with observed absorption for a Lorentzian-broadened source and absorber.

Table 3. γ factor variation with observed transmittance for a Lorentzian-broadened source and absorber

$\frac{\Delta\nu_N \text{ (Source)}}{\Delta\nu_N \text{ (Absorber)}}$	0.1		1.0		3.0		10.0	
lnF	T	γ	T	γ	T	γ	T	γ
-3.2	0.9637	0.999	0.9749	0.994	0.9899	0.992	0.9963	0.990
-2.4	0.9210	0.998	0.9562	0.987	0.9780	0.981	0.9920	0.978
-1.6	0.8331	0.994	0.9064	0.971	0.9526	0.959	0.9826	0.951
-0.8	0.6678	0.986	0.8090	0.934	0.9019	0.910	0.9637	0.897
0.0	0.4133	0.959	0.6453	0.848	0.8117	0.813	0.9288	0.797
0.4	0.2744	0.924	0.5430	0.771	0.7507	0.739	0.9040	0.726
0.8	0.1558	0.843	0.4390	0.665	0.6823	0.653	0.8746	0.654
1.2	0.0767	0.666	0.3460	0.540	0.6115	0.565	0.8412	0.587
1.4	0.0531	0.533	0.3065	0.479	0.5765	0.526	0.8233	0.559
1.6	0.0381	0.393	0.2721	0.425	0.5423	0.492	0.8046	0.535
1.8	0.0292	0.277	0.2425	0.379	0.5091	0.463	0.7851	0.516
2.0	0.0238	0.203	0.2168	0.343	0.4768	0.439	0.7647	0.501
2.2	0.0204	0.164	0.1945	0.315	0.4454	0.418	0.7434	0.488
2.4	0.0179	0.143	0.1749	0.292	0.4151	0.399	0.7211	0.477
2.6	0.0160	0.132	0.1575	0.273	0.3859	0.382	0.6979	0.467
2.8	0.0143	0.125	0.1420	0.257	0.3578	0.367	0.6738	0.457
3.0	0.0128	0.121	0.1281	0.243	0.3308	0.352	0.6487	0.448
3.2	0.0115	0.120	0.1157	0.230	0.3052	0.337	0.6229	0.440

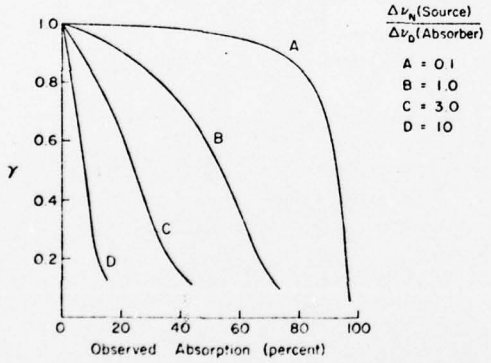

Fig. 5. γ factor variation with observed absorption for a Lorentzian-broadened source and Doppler-broadened absorber.

Fig. 5 and Table 4. Once again in this case of a Doppler-broadened absorber, γ is a steadily changing function of absorption except when γ is near unity. This further indicates the general invalidity of the modified Beer's law for Doppler-broadened absorbers.

(v) *Voigt-broadened source and absorber*

The transmission integral evaluated in this case was

$$I/I_0 = \int_{-\infty}^{\infty} \frac{2}{\Delta\nu_{D_s}} \left(\frac{\ln 2}{\pi}\right)^{1/2} \mathcal{R}W(z) \exp\left[-F\mathcal{R}W(z')/\mathcal{R}W(iy')\right] d\nu, \qquad (26)$$

Table 4. γ factor variation with observed transmittance for a Lorentzian-broadened source and Doppler-broadened absorber

$\frac{\Delta\nu_N \text{ (Source)}}{\Delta\nu_D \text{ (Absorber)}}$	0.1		1.0		3.0		10.0	
lnF	T	γ	T	γ	T	γ	T	γ
-3.2	0.9635	0.999	0.9808	0.993	0.9915	0.988	0.9973	0.986
-2.4	0.9208	0.997	0.9582	0.983	0.9815	0.974	0.9941	0.968
-1.6	0.8326	0.994	0.9109	0.962	0.9604	0.943	0.9873	0.930
-0.8	0.6672	0.984	0.8195	0.913	0.9191	0.874	0.9741	0.852
0.0	0.4138	0.951	0.6692	0.798	0.8488	0.736	0.9513	0.702
0.4	0.2764	0.905	0.5783	0.694	0.8043	0.630	0.9367	0.595
0.8	0.1601	0.801	0.4899	0.555	0.7581	0.507	0.9212	0.476
1.2	0.0833	0.580	0.4159	0.398	0.7154	0.384	0.9065	0.364
1.4	0.0618	0.429	0.3867	0.327	0.6965	0.331	0.9000	0.316
1.6	0.0481	0.286	0.3626	0.267	0.6795	0.286	0.8937	0.277
1.8	0.0402	0.181	0.3430	0.220	0.6642	0.250	0.8880	0.245
2.0	0.0357	0.123	0.3268	0.186	0.6504	0.222	0.8827	0.221
2.2	0.0329	0.095	0.3133	0.161	0.6378	0.201	0.8777	0.201
2.4	0.0308	0.083	0.3017	0.142	0.6262	0.183	0.8730	0.185
2.6	0.0290	0.075	0.2914	0.127	0.6153	0.168	0.8686	0.172
2.8	0.0275	0.068	0.2823	0.115	0.6052	0.156	0.8643	0.161
3.0	0.0262	0.060	0.2741	0.106	0.5956	0.145	0.8602	0.151
3.2	0.0251	0.051	0.2666	0.097	0.5866	0.136	0.8562	0.142

where $\Delta\nu_{D_s}$ is the FWHM of the Gaussian contribution to the source broadening. With $\Delta\nu_{N_s}$ as the FWHM of the Lorentzian contribution to the source broadening, z is given by

$$z = x + iy, \text{ where } x = 2(\nu - \nu_0)(\ln 2)^{1/2}/\Delta\nu_{D_s} \text{ and } y = \Delta\nu_{N_s}(\ln 2)^{1/2}/\Delta\nu_{D_s}$$

while, for the absorber, $z' = x' + iy'$, where $x' = 2(\nu - \nu_0)(\ln 2)^{1/2}/\Delta\nu_{D_a}$ and $y' = \Delta\nu_{N_a}(\ln 2)^{1/2}/\Delta\nu_{D_a}$. To allow comparison of the results with those for Gaussian and Lorentzian-broadened sources, we use the Voigt profile normalized to unity at the line centre in the second exponential factor in eqn (26). This ensures that this second exponential factor becomes e^{-F} at the line centre, as before. To evaluate the real part of the error function for complex argument, we used the very accurate algorithm described by REICHEL.[28] However, as pointed out by Reichel and confirmed by us, this algorithm was generally unsuitable when either $x^2 > 49$ or when simultaneously $x^2 < 49$ and $1/4y^2 \ll 1$. For these values of x and y, we used the very satisfactory numerical expressions for $\mathcal{R}W(z)$ given by Gautschi in Ref. (3). Alternative algorithms for $\mathcal{R}W(z)$ described by WHITING[29] and HARSTAD[30] were insufficiently accurate and not markedly more convenient to use.

Some typical results obtained from eqn (26) are shown in Fig. 6 and Table 5. The figure shows the γ-factor dependence on absorption for sources and absorbers with Lorentzian width/Gaussian width ratios of unity. These curves illustrate the behaviour of sources and absorbers with line shapes intermediate between those combinations considered previously in (i)–(iv). Again, Fig. 6 illustrates the tendency of γ to change more slowly with absorption, for large source linewidth/absorber linewidth ratios, when the absorber has a substantial degree of Lorentzian character.

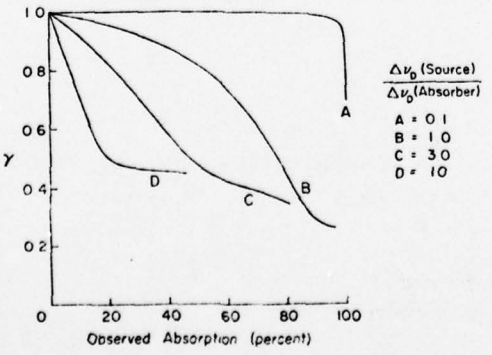

Fig. 6. γ factor variation with observed absorption for a Voigt-broadened source and absorber with equal Lorentzian and Gaussian widths.

Table 5. γ factor variation with observed transmittance for a Voigt-broadened source and absorber each with Lorentzian width/Gaussian width = 1

$\frac{\Delta\nu_D \text{ (Source)}}{\Delta\nu_D \text{ (Absorber)}}$	0.1		1.0		3.0		10.0	
lnF	T	γ	T	γ	T	γ	T	γ
-3.2	0.9612	1.000	0.9765	0.995	0.9886	0.991	0.9961	0.989
-2.4	0.9158	1.000	0.9487	0.990	0.9751	0.981	0.9914	0.975
-1.6	0.8223	0.999	0.8996	0.977	0.9466	0.958	0.9815	0.946
-0.8	0.6472	0.998	0.7778	0.946	0.8899	0.908	0.9615	0.886
0.0	0.3805	0.995	0.5912	0.870	0.7907	0.806	0.9255	0.774
0.4	0.2373	0.992	0.4772	0.798	0.7249	0.728	0.9005	0.698
0.8	0.1179	0.985	0.3649	0.692	0.6527	0.637	0.8716	0.617
1.2	0.0422	0.969	0.2692	0.557	0.5796	0.547	0.8398	0.547
1.4	0.0214	0.953	0.2306	0.489	0.5442	0.509	0.8230	0.520
1.6	0.0095	0.927	0.1983	0.428	0.5098	0.478	0.8056	0.500
1.8	0.0037	0.882	0.1716	0.379	0.4765	0.454	0.7875	0.486
2.0	0.0013	0.815	0.1493	0.342	0.4441	0.435	0.7685	0.477
2.2	0.0004	0.732	0.1305	0.315	0.4125	0.421	0.7485	0.471
2.4	0.0001	0.664	0.1143	0.297	0.3816	0.410	0.7274	0.467
2.6	0.0000	0.635	0.1001	0.284	0.3515	0.400	0.7051	0.464
2.8	0.0000	0.641	0.0875	0.275	0.3222	0.391	0.6815	0.462
3.0	0.0000	0.663	0.0763	0.268	0.2939	0.381	0.6567	0.460
3.2	0.0000	0.691	0.0662	0.264	0.2667	0.372	0.6307	0.457

(vi) *Model one-dimensional single layer self-reversed Doppler-broadened source and Doppler-broadened absorber*

Sources used in atomic absorption spectroscopy frequently have lineshapes modified by reabsorption. A simple model of such a source is one where the source is extended in the direction in which emission passes out to the absorber, is Doppler-broadened at a uniform temperature and contains a uniform concentration of atoms in the lower level of the emitting transition. It is assumed that radiation emitted towards the absorber, if reabsorbed, has negligibly small probability of being reemitted in the direction of the absorber. A capillary discharge source viewed axially as a source of ion-resonance transitions could satisfy these conditions.

Such a source can be viewed as a one-dimensional, uniform, single layer. If the absorption coefficient at frequency ν within the source is $\alpha(\nu)$, its unreversed normalized lineshape function is $g(\nu)$ and its length is L, then its normalized self-reversed lineshape function is

$$g_s(\nu) = \frac{\sigma[1 - e^{-kNLg(\nu)}]}{1 - e^{-k_0 NL}}, \tag{27}$$

where the normalization factor σ is given by the expression

$$\sigma = (1 - e^{-k_0 NL})\left[\sum_{n=1}^{\infty} \frac{(-1)^{n+1}\pi^{1/2} D^n \Delta\nu_{D_s}}{n!2(n \ln 2)^{1/2}}\right]^{-1}. \tag{28}$$

Here D is the optical thickness of the source which, for a Doppler-broadened, unreversed source lineshape, is defined by

$$kNLg(\nu) = D \exp\{-[2(\nu - \nu_0)/\Delta\nu_{D_s}]^2 \ln 2\}. \tag{29}$$

For this type of source and a Doppler-broadened absorber, we have evaluated the transmission integral

$$I/I_0 = \int_{-\infty}^{\infty} \left(\frac{\sigma}{1 - e^{-k_0 NL}}\right)\{1 - \exp[-D \exp\{-[2(\nu - \nu_0)/\Delta\nu_s]^2 \ln 2\}]\}$$

$$\times \exp[-F \exp\{-[2(\nu - \nu_0)/\Delta\nu_a]^2 \ln 2\}]\, d\nu \tag{30}$$

for a wide range of values of F, D and source linewidth/absorber linewidth ratios. Some typical results from these computations are given in Tables 6 and 7. Once again in these cases, where the absorber is Doppler-broadened, except for $\gamma \sim 1$, γ is not a slowly varying function of absorption, invalidating use of the modified Beer's law in this case.

Table 6. γ factor variation with observed transmittance for a model one-dimensional single layer self-reversed Doppler-broadened source (1LSRS) with optical thickness $D = 1$ and a Doppler-broadened absorber

$\Delta\nu_D$ (Source) / $\Delta\nu_D$ (Absorber)	0.1		1.0		3.0		10.0	
lnF	T	γ	T	γ	T	γ	T	γ
-3.2	0.9603	1.000	0.9731	0.997	0.9887	0.990	0.9965	0.986
-2.4	0.9138	1.000	0.9413	0.993	0.9753	0.978	0.9924	0.969
-1.6	0.8181	1.000	0.8749	0.985	0.9471	0.951	0.9836	0.933
-0.8	0.6397	1.000	0.7465	0.965	0.8917	0.892	0.9665	0.856
0.0	0.3700	1.000	0.5350	0.916	0.7972	0.768	0.9370	0.708
0.4	0.2269	1.000	0.4073	0.866	0.7368	0.672	0.9180	0.603
0.8	0.1094	1.000	0.2833	0.787	0.6736	0.554	0.8980	0.484
1.2	0.0369	1.000	0.1810	0.671	0.6143	0.435	0.8789	0.372
1.4	0.0178	1.000	0.1415	0.604	0.5877	0.382	0.8702	0.324
1.6	0.0073	1.000	0.1101	0.538	0.5633	0.337	0.8621	0.285
1.8	0.0024	1.000	0.0857	0.477	0.5413	0.301	0.8547	0.253
2.0	0.0006	1.000	0.0670	0.426	0.5210	0.273	0.8477	0.228
2.2	0.0001	1.000	0.0526	0.385	0.5023	0.250	0.8412	0.208
2.4	0.0000	1.000	0.0416	0.353	0.4849	0.232	0.8350	0.192
2.6	0.0000	0.999	0.0330	0.326	0.4685	0.217	0.8292	0.179
2.8	0.0000	0.999	0.0262	0.304	0.4530	0.204	0.8235	0.168
3.0	0.0000	0.999	0.0208	0.285	0.4383	0.192	0.8181	0.158
3.2	0.0000	0.999	0.0166	0.268	0.4244	0.183	0.8128	0.149

Table 7. γ factor variation with observed transmittance for a 1LSRS with optical thickness $D = 10$ and Doppler-broadened absorber

$\Delta\nu_D$ (Source) / $\Delta\nu_D$ (Absorber)	0.1		1.0		3.0		10.0	
lnF	T	γ	T	γ	T	γ	T	γ
-3.2	0.9605	1.000	0.9793	0.995	0.9928	0.988	0.9979	0.985
-2.4	0.9141	1.000	0.9547	0.989	0.9843	0.974	0.9953	0.968
-1.6	0.8189	1.000	0.8831	0.976	0.9664	0.942	0.9899	0.929
-0.8	0.6411	1.000	0.8020	0.945	0.9312	0.874	0.9794	0.850
0.0	0.3718	1.000	0.6303	0.874	0.8707	0.738	0.9612	0.699
0.4	0.2285	1.000	0.5215	0.810	0.8318	0.637	0.9495	0.593
0.8	0.1106	1.000	0.4044	0.724	0.7906	0.520	0.9372	0.475
1.2	0.0374	1.000	0.3070	0.620	0.7513	0.406	0.9254	0.363
1.4	0.0181	1.000	0.2627	0.563	0.7333	0.357	0.9200	0.316
1.6	0.0074	1.000	0.2237	0.521	0.7167	0.316	0.9150	0.277
1.8	0.0025	1.000	0.1897	0.489	0.7012	0.283	0.9104	0.246
2.0	0.0007	0.999	0.1605	0.447	0.6869	0.257	0.9060	0.222
2.2	0.0001	0.999	0.1352	0.420	0.6734	0.237	0.9020	0.203
2.4	0.0000	0.999	0.1135	0.396	0.6606	0.220	0.8982	0.187
2.6	0.0000	0.999	0.0948	0.376	0.6484	0.206	0.8945	0.174
2.8	0.0000	0.999	0.0789	0.358	0.6366	0.195	0.8910	0.163
3.0	0.0000	0.998	0.0653	0.341	0.6253	0.184	0.8876	0.154
3.2	0.0000	0.998	0.0539	0.325	0.6144	0.175	0.8843	0.145

(vii) *Model one-dimensional single layer self-reversed Doppler-broadened source and Lorentzian-broadened absorber*

Here we have used the same source lineshape function as in (vi) and evaluated the transmission integral

$$I/I_0 = \int_{-\infty}^{\infty} \left(\frac{\sigma}{1-e^{-kNL}}\right)(1-\exp[-D\exp\{-[2/(\nu-\nu_0)/\Delta\nu_{D_s}]^2\ln 2\}]) \times \exp[-F\{1+[2/(\nu-\nu_0)/\Delta\nu_{N_a}]^2\}^{-1}]\,d\nu. \quad (31)$$

Some typical results are given in Tables 8 and 9. There is again a tendency for γ to vary slowly with absorption for large values of the linewidth ratio, for this absorber with a Lorentzian lineshape.

(viii) *Model one-dimensional three-layer self-reversed Doppler-broadened sources and Doppler-broadened absorbers*

The one-dimensional, one-layer, model of a self-reversed source just discussed is inadequate to describe most neutral resonance line sources used in atomic absorption spectroscopy. BRAUN and CARRINGTON[33] have proposed an improved two-layer model of a one-dimensional self-reversed source which is a better approximation to reality. They treat the source as consisting of 2 layers, an emitting layer and a reversing layer, each Doppler-broadened at different temperatures, extended in the direction of emission. As before, a photon emitted

Table 8. γ factor variation with observed transmittance for a 1LSRS with optical thickness $D = 1$ and Lorentzian-broadened absorber

$\Delta\nu_D$ (Source) / $\Delta\nu_N$ (Absorber)	0.1		1.0		3.0		10.0	
lnF	T	γ	T	γ	T	γ	T	γ
-3.2	0.9604	1.000	0.9730	0.998	0.9864	0.994	0.9952	0.991
-2.4	0.9140	1.000	0.9409	0.995	0.9703	0.986	0.9894	0.979
-1.6	0.8185	1.000	0.8739	0.989	0.9360	0.969	0.9772	0.955
-0.8	0.6404	1.000	0.7436	0.975	0.8674	0.933	0.9522	0.905
0.0	0.3710	1.000	0.5265	0.943	0.7449	0.859	0.9061	0.812
0.4	0.2278	1.000	0.3935	0.912	0.6616	0.802	0.8732	0.749
0.8	0.1101	1.000	0.2624	0.866	0.5679	0.735	0.8338	0.681
1.2	0.0372	1.000	0.1525	0.802	0.4705	0.667	0.7889	0.620
1.4	0.0179	1.000	0.1100	0.765	0.4225	0.638	0.7646	0.595
1.6	0.0074	1.000	0.0763	0.727	0.3757	0.613	0.7391	0.576
1.8	0.0025	1.000	0.0510	0.692	0.3307	0.594	0.7123	0.561
2.0	0.0007	0.999	0.0328	0.662	0.2876	0.579	0.6842	0.550
2.2	0.0001	0.999	0.0202	0.638	0.2468	0.568	0.6547	0.542
2.4	0.0000	0.999	0.0119	0.619	0.2086	0.560	0.6237	0.536
2.6	0.0000	0.999	0.0066	0.605	0.1732	0.554	0.5913	0.531
2.8	0.0000	0.999	0.0035	0.593	0.1410	0.549	0.5574	0.528
3.0	0.0000	0.998	0.0017	0.582	0.1124	0.545	0.5223	0.525
3.2	0.0000	0.997	0.0008	0.573	0.0873	0.542	0.4861	0.523
3.6							0.4111	0.521
4.0							0.3346	0.520
4.4							0.2598	0.520
4.8							0.1903	0.520
5.2							0.1297	0.521
5.6							0.0808	0.521
6.0							0.0451	0.522
6.4							0.0220	0.521
6.8							0.0091	0.521
7.2							0.0031	0.520

Table 9. γ factor variation with observed transmittance for a 1LSRS with optical thickness $D = 10$ and Lorentzian-broadened absorber

$\Delta\nu_D$ (Source) / $\Delta\nu_N$ (Absorber)	0.1		1.0		3.0		10.0	
lnF	T	γ	T	γ	T	γ	T	γ
-3.2	0.9606	1.000	0.9780	0.997	0.9906	0.993	0.9970	0.990
-2.4	0.9145	1.000	0.9519	0.993	0.9793	0.984	0.9932	0.978
-1.6	0.8196	1.000	0.8967	0.985	0.9553	0.964	0.9854	0.953
-0.8	0.6423	1.000	0.7879	0.966	0.9068	0.924	0.9693	0.901
0.0	0.3734	1.000	0.6000	0.924	0.8182	0.845	0.9394	0.807
0.4	0.2300	1.000	0.4786	0.889	0.7558	0.789	0.9178	0.744
0.8	0.1117	1.000	0.3511	0.842	0.6828	0.727	0.8915	0.679
1.2	0.0380	1.000	0.2326	0.788	0.6022	0.670	0.8609	0.621
1.4	0.0184	0.999	0.1814	0.761	0.5600	0.647	0.8441	0.599
1.6	0.0076	0.999	0.1370	0.736	0.5169	0.629	0.8260	0.582
1.8	0.0026	0.999	0.0999	0.716	0.4731	0.616	0.8068	0.569
2.0	0.0007	0.999	0.0701	0.700	0.4289	0.607	0.7862	0.560
2.2	0.0001	0.999	0.0470	0.687	0.3845	0.602	0.7641	0.554
2.4	0.0000	0.998	0.0300	0.678	0.3402	0.600	0.7404	0.550
2.6	0.0000	0.998	0.0180	0.670	0.2965	0.598	0.7150	0.547
2.8	0.0000	0.997	0.0101	0.662	0.2541	0.599	0.6878	0.546
3.0	0.0000	0.996	0.0053	0.654	0.2134	0.600	0.6587	0.546
3.2	0.0000	0.995	0.0025	0.646	0.1753	0.601	0.6277	0.546
3.6							0.5602	0.549
4.0							0.4858	0.554
4.4							0.4059	0.561
4.8							0.3233	0.568
5.2							0.2420	0.577
5.6							0.1672	0.585
6.0							0.1041	0.593
6.4							0.0567	0.599
6.8							0.0261	0.602
7.							0.0097	0.601

towards the absorption cell, if reabsorbed, is assumed to have negligibly small probability of once more being emitted in this direction. The frequency dependence of such a model is

$$g_2(\nu) \propto (1 - \exp[-D_1 \exp\{-[2(\nu - \nu_0)/\Delta\nu_{D_1}]^2 \ln 2\}]) \exp[-D_2 \exp\{-[2(\nu - \nu_0)/\Delta\nu_{D_2}]^2 \ln 2\}], \tag{32}$$

where D_1 and D_2 are the optical thicknesses of the two layers and $\Delta\nu_{D_1}$ and $\Delta\nu_{D_2}$ are their respective Doppler widths. An example of such a lineshape is shown in Fig. 7 at I_B, which is appropriate for $D_1 = D_2 = 1$ and $(\Delta\nu_{D_1}/\Delta\nu_{D_2})^2 = 1.5$. We have extended this model to include a third layer, which we call the absorbing layer, which further reverses the source lineshape, and

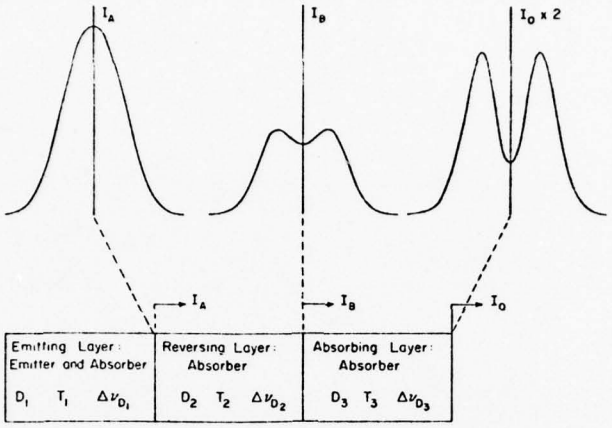

Fig. 7. Development of one-dimensional, three-layer, self-reversed Doppler-broadened source line-shape (3LSRS). The optical thickness, temperature and unreversed Doppler FWHM of each layer are D_1, T_1, $\Delta\nu_{D_1}$; D_2, T_2, $\Delta\nu_{D_2}$; D_3, T_3, $\Delta\nu_{D_3}$ respectively. The figure is appropriate to $D_1:D_2:D_3 = 1:1:1$ and $T_1:T_2:T_3 = 15:20:3$.

gives lineshapes which resemble experimentally observed self-reversed lineshapes well. This model gives lineshapes

$$g_3(\nu) = \beta\{1 - \exp[-D_1 \exp\{-[2(\nu-\nu_0)/\Delta\nu_{D_1}]^2 \ln 2\}]\} \times \{1 - \exp[-D_2 \exp\{-[2(\nu-\nu_0)/\Delta\nu_{D_2}]^2 \ln 2\}]\} \exp[-D_3 \exp\{-[2(\nu-\nu_0)/\Delta\nu_{D_3}]^2 \ln 2\}], \quad (33)$$

where β is a normalization factor. An example of such a line shape is shown in Fig. 7 at I_0. Physically, the three layers in such a model correspond to the hot emitting region of a resonance lamp, the hot layer of non-emitting gas between this emitting region and the lamp window, and the cooler layer of absorbing gas in contact with the window.

Using the above model, we have evaluated the transmission integral

$$I/I_0 = \int_{-\infty}^{\infty} g_3(\nu) \exp(-F \exp[-F \exp\{-[2(\nu-\nu_0)/\Delta\nu_{D_a}]^2 \ln 2\}])\, d\nu \quad (34)$$

for a variety of self-reversed sources with different parameter ratios $D_1:D_2:D_3$ and $T_1:T_3:T_3$ for a wide range of values of F and the fundamental source/absorber linewidth ratio $\Delta\nu_{D_1}/\Delta\nu_{D_a}$. These self-reversed source lineshapes ranged from small self-reversal ($D_1 = 0.1$, $D_2 = 0.1$, $D_3 = 1$; $T_1:T_2:T_3 = 15:10:3$) to extreme self-reversal ($D_1 = 100$, $D_2 = 1$, $D_3 = 100$; $T_1:T_2:T_3 = 15:10:3$). Results showing the variation of γ with absorption are given in Fig. 8 and Tables 11–14. In no

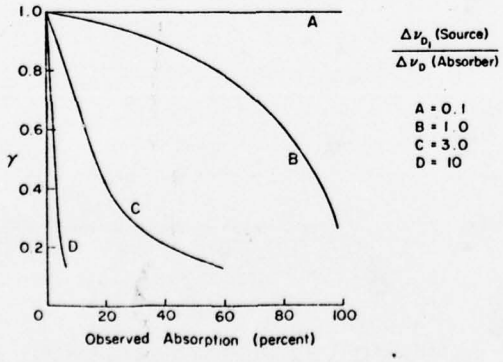

Fig. 8. γ factor variation with observed absorption for 3LSRS ($D_1:D_2:D_3 = 1:1:1$; $T_1:T_2:T_3 = 15:10:3$) and Doppler-broadened absorber.

Table 10. γ factor variation with observed transmittance for a model one-dimensional three-layer self-reversed Doppler-broadened source (3LSRS) with $D_1 : D_2 : D_3 = 0.1 : 0.1 : 1$ and $T_1 : T_2 : T_3 = 30 : 10 : 3$ and a Doppler-broadened absorber

$\frac{\Delta\nu_D \text{ (Source)}}{\Delta\nu_D \text{ (Absorber)}}$	0.1		1.0		3.0		10.0	
lnF	T	γ	T	γ	T	γ	T	γ
-3.2	0.9603	1.000	0.9748	0.997	0.9921	0.990	0.9982	0.986
-2.4	0.9138	1.000	0.9450	0.994	0.9828	0.978	0.9960	0.968
-1.6	0.8182	1.000	0.8825	0.986	0.9629	0.952	0.9914	0.930
-0.8	0.6399	1.000	0.7605	0.967	0.9233	0.895	0.9824	0.852
0.0	0.3703	1.000	0.5560	0.921	0.8535	0.782	0.9668	0.705
0.4	0.2272	1.000	0.4296	0.876	0.8066	0.697	0.9567	0.602
0.8	0.1096	1.000	0.3037	0.804	0.7548	0.598	0.9458	0.488
1.2	0.0369	1.000	0.1962	0.700	0.7021	0.497	0.9352	0.381
1.4	0.0178	1.000	0.1536	0.637	0.6766	0.451	0.9303	0.336
1.6	0.0073	1.000	0.1191	0.572	0.6521	0.411	0.9256	0.299
1.8	0.0025	1.000	0.0920	0.509	0.6286	0.376	0.9212	0.269
2.0	0.0006	1.000	0.0712	0.454	0.6063	0.346	0.9171	0.245
2.2	0.0001	1.000	0.0554	0.408	0.5849	0.321	0.9131	0.227
2.4	0.0000	1.000	0.0433	0.370	0.5644	0.299	0.9092	0.211
2.6	0.0000	0.999	0.0340	0.339	0.5449	0.280	0.9055	0.199
2.8	0.0000	0.999	0.0268	0.314	0.5261	0.263	0.9019	0.188
3.0	0.0000	0.999	0.0212	0.292	0.5082	0.248	0.8983	0.178
3.2	0.0000	0.999	0.0168	0.274	0.4910	0.234	0.8948	0.170

Table 11. γ factor variation with observed transmittance for a 3LSRS ($D_1 : D_2 : D_3 = 1 : 1 : 1$; $T_1 : T_2 : T_3 = 15 : 10 : 3$) and Doppler-broadened absorber

$\frac{\Delta\nu_D \text{ (Source)}}{\Delta\nu_D \text{ (Absorber)}}$	0.1		1.0		3.0		10.0	
lnF	T	γ	T	γ	T	γ	T	γ
-3.2	0.9604	1.000	0.9790	0.997	0.9956	0.989	0.9991	0.9851
-2.4	0.9140	1.000	0.9540	0.992	0.9903	0.997	0.9981	0.9672
-1.6	0.8186	1.000	0.9012	0.983	0.9791	0.949	0.9960	0.9287
-0.8	0.6406	1.000	0.7968	0.962	0.9566	0.891	0.9918	0.8492
0.0	0.3712	1.000	0.6161	0.912	0.9158	0.781	0.9845	0.7012
0.4	0.2280	1.000	0.4992	0.866	0.8875	0.702	0.9797	0.5985
0.8	0.1102	1.000	0.3766	0.799	0.8551	0.612	0.9746	0.4862
1.2	0.0373	1.000	0.2636	0.708	0.8202	0.523	0.9695	0.3814
1.4	0.0180	1.000	0.2153	0.655	0.8024	0.483	0.9671	0.3377
1.6	0.0074	1.000	0.1736	0.600	0.7847	0.447	0.9649	0.3014
1.8	0.0025	1.000	0.1389	0.546	0.7671	0.416	0.9627	0.2724
2.0	0.0007	1.000	0.1106	0.496	0.7496	0.389	0.9607	0.2495
2.2	0.0001	1.000	0.0879	0.452	0.7323	0.365	0.9587	0.2313
2.4	0.0000	0.999	0.0698	0.414	0.7152	0.344	0.9568	0.2164
2.6	0.0000	0.999	0.0555	0.380	0.6983	0.325	0.9549	0.2038
2.8	0.0000	0.999	0.0441	0.352	0.6817	0.308	0.9531	0.1931
3.0	0.0000	0.999	0.0352	0.327	0.6653	0.293	0.9513	0.1837
3.2	0.0000	0.999	0.0280	0.306	0.6491	0.278	0.9495	0.1754

Table 12. γ factor variation with observed transmittance for a 3LSRS ($D_1 : D_2 : D_3 = 1 : 1 : 1$; $T_1 : T_2 : T_3 = 30 : 10 : 3$) and Doppler-broadened absorber

$\frac{\Delta\nu_D \text{ (Source)}}{\Delta\nu_D \text{ (Absorber)}}$	0.1		1.0		3.0		10.0	
lnF	T	γ	T	γ	T	γ	T	γ
-3.2	0.9604	1.000	0.9801	0.996	0.9956	0.988	0.9990	0.985
-2.4	0.9141	1.000	0.9563	0.992	0.9903	0.974	0.9977	0.967
-1.6	0.8188	1.000	0.9063	0.981	0.9792	0.944	0.9952	0.928
-0.8	0.6409	1.000	0.8070	0.958	0.9570	0.881	0.9901	0.847
0.0	0.3715	1.000	0.6343	0.904	0.9174	0.759	0.9813	0.700
0.4	0.2282	1.000	0.5216	0.856	0.8907	0.673	0.9756	0.592
0.8	0.1104	1.000	0.4022	0.788	0.8606	0.576	0.9695	0.477
1.2	0.0374	1.000	0.2899	0.699	0.8293	0.482	0.9636	0.369
1.4	0.0180	1.000	0.2408	0.649	0.8137	0.442	0.9609	0.324
1.6	0.0074	1.000	0.1976	0.598	0.7984	0.407	0.9583	0.286
1.8	0.0025	1.000	0.1608	0.550	0.7833	0.378	0.9559	0.257
2.0	0.0007	1.000	0.1300	0.504	0.7684	0.353	0.9537	0.233
2.2	0.0001	1.000	0.1047	0.463	0.7538	0.333	0.9515	0.214
2.4	0.0000	0.999	0.0841	0.427	0.7392	0.315	0.9494	0.199
2.6	0.0000	0.999	0.0675	0.395	0.7248	0.300	0.9474	0.187
2.8	0.0000	0.999	0.0540	0.367	0.7105	0.286	0.9455	0.176
3.0	0.0000	0.999	0.0433	0.342	0.6964	0.273	0.9436	0.166
3.2	0.0000	0.998	0.0346	0.320	0.6824	0.262	0.9418	0.158
3.6					0.6548	0.241		
4.0					0.6278	0.224		
4.4					0.6015	0.209		
4.8					0.5759	0.195		
5.2					0.5511	0.183		
5.6					0.5271	0.172		
6.0					0.5038	0.163		
6.4					0.4814	0.154		
6.8					0.4598	0.146		
7.2					0.4391	0.139		

Table 13. γ factor variation with observed transmittance for a 3LSRS ($D_1:D_2:D_3 = 10:1:10$; $T_1:T_2:T_3 = 15:10:3$) and Doppler-broadened absorber

$\frac{\Delta\nu_D \text{ (Source)}}{\Delta\nu_D \text{ (Absorber)}}$	0.1		1.0		3.0		10.0	
lnF	T	γ	T	γ	T	γ	T	γ
-3.2	0.9608	1.000	0.9904	0.997	0.9979	0.998	1.0000	0.987
-2.4	0.9148	1.000	0.9789	0.993	0.9998	0.996	1.0000	0.971
-1.6	0.8202	1.000	0.9540	0.985	0.9996	0.992	1.0000	0.937
-0.8	0.6433	1.000	0.9020	0.968	0.9992	0.983	1.0000	0.869
0.0	0.3747	1.000	0.8013	0.930	0.9983	0.964	1.0000	0.746
0.4	0.2312	1.000	0.7259	0.897	0.9974	0.949	1.0000	0.663
0.8	0.1125	1.000	0.6334	0.852	0.9963	0.930	1.0000	0.576
1.2	0.0384	1.000	0.5282	0.791	0.9949	0.904	1.0000	0.498
1.4	0.0187	1.000	0.4734	0.755	0.9937	0.889	1.0000	0.466
1.6	0.0077	1.000	0.4191	0.716	0.9925	0.872	1.0000	0.441
1.8	0.0026	1.000	0.3666	0.675	0.9910	0.854	1.0000	0.420
2.0	0.0007	0.999	0.3172	0.633	0.9894	0.834	1.0000	0.405
2.2	0.0001	0.999	0.2716	0.592	0.9874	0.813	1.0000	0.392
2.4	0.0000	0.999	0.2306	0.553	0.9852	0.791	1.0000	0.382
2.6	0.0000	0.999	0.1942	0.516	0.9827	0.767	1.0000	0.374
2.8	0.0000	0.999	0.1625	0.483	0.9799	0.743	1.0000	0.367
3.0	0.0000	0.998	0.1351	0.452	0.9767	0.719	1.0000	0.361
3.2	0.0000	0.998	0.1118	0.424	0.9732	0.693	1.0000	0.346

Table 14. γ factor variation with observed transmittance for a 3LSRS ($D_1:D_2:D_3 = 100:1:100$; $T_1:T_2:T_3 = 15:10:3$) and Doppler-broadened absorber

$\frac{\Delta\nu_D \text{ (Source)}}{\Delta\nu_D \text{ (Absorber)}}$	0.1		0.5		1.0		3.0	
lnF	T	γ	T	γ	T	γ	T	γ
-3.2	0.9612	1.000	0.9798	0.999	0.9958	0.998	1.0000	1.000
-2.4	0.9157	1.000	0.9556	0.997	0.9908	0.995	1.0000	1.000
-1.6	0.8221	1.000	0.9042	0.994	0.9797	0.988	1.0000	1.000
-0.8	0.6466	1.000	0.8004	0.987	0.9559	0.974	1.0000	1.000
0.0	0.3789	1.000	0.6136	0.971	0.9070	0.944	1.0000	1.000
0.4	0.2351	1.000	0.4872	0.956	0.8676	0.918	1.0000	0.999
0.8	0.1154	1.000	0.3493	0.933	0.8151	0.882	1.0000	0.999
1.2	0.0399	1.000	0.2180	0.899	0.7487	0.832	0.9999	0.998
1.4	0.0196	1.000	0.1615	0.878	0.7104	0.802	0.9999	0.998
1.6	0.0082	0.999	0.1138	0.852	0.6694	0.768	0.9999	0.997
1.8	0.0028	0.999	0.0760	0.822	0.6263	0.732	0.9999	0.997
2.0	0.0008	0.999	0.0479	0.790	0.5817	0.693	0.9999	0.996
2.2	0.0002	0.999	0.0285	0.754	0.5367	0.655	0.9999	0.995
2.4	0.0000	0.999	0.0160	0.716	0.4920	0.617	0.9998	0.994
2.6	0.0000	0.998	0.0085	0.676	0.4482	0.581	0.9998	0.993
2.8	0.0000	0.998	0.0042	0.634	0.4060	0.549	0.9997	0.991
3.0	0.0000	0.997	0.0020	0.590	0.3656	0.521	0.9997	0.989
3.2	0.0000	0.996	0.0009	0.545	0.3274	0.495	0.9996	0.987

case does γ approach a nearly constant value over any significant range of absorption, except when $\Delta\nu_{D_1}/\Delta\nu_{D_a} \ll 1$ and $\gamma \to 1$. This once again shows the invalid nature of the modified Beer's law for γ factors < 1 when the absorber is Doppler-broadened.

(ix) *Model one-dimensional three-layer self-reversed Doppler-broadened sources and Lorentzian-broadened absorbers*

Using the same self-reversed lineshape function as in Section (viii), we have evaluated the transmission integral

$$I/I_0 = \int_{-\infty}^{\infty} g_3(\nu) \exp\left[-F\{1 + [2(\nu - \nu_0)/\Delta\nu_{N_a}]^2\}^{-1}\right] d\nu \tag{35}$$

for a variety of source parameter ratios $D_1:D_2:D_3$ and $T_1:T_2:T_3$ and a wide range of F and the fundamental source/absorber linewidth ratio $\Delta\nu_{D_1}/\Delta\nu_{N_a}$. Typical results are given in Fig. 9 and Tables 15–19. These results show that γ is a more slowly varying function of absorption than is the case for Doppler-broadened absorbers. Furthermore, for large values of the linewidth ratio $\Delta\nu_{D_1}/\Delta\nu_{N_a}$, γ approaches a fairly constant value over a wide range of absorptions. A number of the curves tabulated in Tables 15–19 could not be extended to large values of absorption for the range of values of F used. This occurs particularly for heavily self-reversed sources and absorbers when the ratio $\Delta\nu_{D_1}/\Delta\nu_{N_a}$ is large; in these cases, almost all the emission from the source lies outside the region of significant absorption.

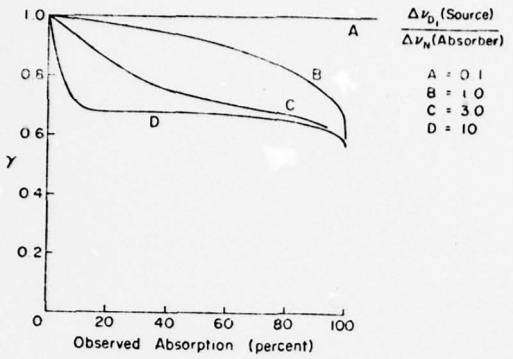

Fig. 9. γ factor variation with observed absorption for 3LSRS ($D_1:D_2:D_3 = 1:1:1$; $T_1:T_2:T_3 = 15:10:3$) and Lorentzian-broadened absorber.

Table 15. γ factor variation with observed transmittance for a 3LSRS ($D_1:D_2:D_3) = 0.1:0.1:1$; $T_1:T_2:T_3 = 30:10:3$) and Lorentzian-br adened absorber

$\frac{\Delta\nu_D(\text{Source})}{\Delta\nu_N(\text{Absorber})}$	0.1		1.0		3.0		10.0	
lnF	T	γ	T	γ	T	γ	T	γ
-3.2	0.9604	1.000	0.9747	0.998	0.9893	0.994	0.9970	0.991
-2.4	0.9140	1.000	0.9446	0.996	0.9765	0.988	0.9934	0.981
-1.6	0.8187	1.000	0.8814	0.990	0.9491	0.973	0.9857	0.960
-0.8	0.6407	1.000	0.7574	0.977	0.8933	0.943	0.9698	0.916
0.0	0.3713	1.000	0.5472	0.948	0.7897	0.883	0.9395	0.838
0.4	0.2281	1.000	0.4152	0.922	0.7156	0.839	0.9168	0.788
0.8	0.1103	1.000	0.2818	0.882	0.6277	0.788	0.8884	0.737
1.2	0.0373	1.000	0.1664	0.827	0.5299	0.736	0.8537	0.693
1.4	0.0180	1.000	0.1205	0.794	0.4742	0.712	0.8338	0.677
1.6	0.0074	1.000	0.0837	0.759	0.4282	0.690	0.8121	0.665
1.8	0.0025	1.000	0.0557	0.724	0.3776	0.671	0.7885	0.655
2.0	0.0007	0.999	0.0355	0.692	0.3283	0.654	0.7627	0.649
2.2	0.0001	0.999	0.0217	0.663	0.2810	0.639	0.7346	0.644
2.4	0.0000	0.999	0.0126	0.639	0.2363	0.625	0.7041	0.640
2.6	0.0000	0.999	0.0069	0.620	0.1950	0.613	0.6712	0.636
2.8	0.0000	0.999	0.0036	0.603	0.1576	0.601	0.6358	0.633
3.0	0.0000	0.998	0.0017	0.590	0.1244	0.591	0.5981	0.629
3.2	0.0000	0.997	0.0008	0.578	0.0958	0.581	0.5583	0.625
3.6							0.4735	0.616
4.0							0.3846	0.605
4.4							0.2966	0.593
4.8							0.2147	0.580
5.2							0.1440	0.568
5.6							0.0881	0.556
6.0							0.0482	0.547
6.4							0.0231	0.538
6.8							0.0094	0.531
7.2							0.0031	0.526

(x) *Model one-dimensional three-layer self-reversed Doppler-broadened source and Voigt-broadened absorber*

The transmission integral we have evaluated in this case is

$$I/I_0 = \int_{-\infty}^{\infty} g_3(\nu) \exp\left[-F\mathcal{R}W(z')/\mathcal{R}W(iy')\right] d\nu. \tag{36}$$

Results from these computations for a Voigt-broadened absorber whose Lorentzian width/Gaussian width ratio was unity are given in Table 20. Again, for large source/absorber linewidth ratios, γ becomes nearly constant or slowly varying for this absorber, which has a substantial degree of Lorentzian broadening. It seems to be a general result that, for Lorentzian absorbers and large source/absorber linewidth ratios, γ may become nearly constant or at least more slowly varying than for other types of absorption lineshape.

DISCUSSION AND CONCLUSIONS

Figures 1–9 and Tables 1–20† represent a comprehensive survey of the various types of source/absorber lineshape combinations likely to be encountered in time-resolved atomic

†Graphical presentation of all the γ factor/observed absorption curves tabulated in Tables 1–20 and the curves of growth from which they were derived are available.[32]

Table 16. γ factor variation with observed transmittance for a 3LSRS ($D_1:D_2:D_3 = 1:1:1$; $T_1:T_2:T_3 = 15:10:3$) and Lorentzian-broadened absorber

$\Delta\nu_D$ (Source) / $\Delta\nu_N$ (Absorber)	0.1		1.0		3.0		10.0	
lnF	T	γ	T	γ	T	γ	T	γ
-3.2	0.9606	1.000	0.9740	0.998	0.9828	0.994	0.9882	0.991
-2.4	0.9144	1.000	0.9539	0.995	0.9840	0.987	0.9900	0.981
-1.6	0.8195	1.000	0.9008	0.988	0.9653	0.973	0.9814	0.960
-0.8	0.6420	1.000	0.7950	0.974	0.9265	0.942	0.9617	0.916
0.0	0.3730	1.000	0.6087	0.944	0.8523	0.887	0.9113	0.841
0.4	0.2247	1.000	0.4854	0.914	0.7970	0.849	0.8740	0.794
0.8	0.1114	1.000	0.3534	0.884	0.7280	0.808	0.8309	0.747
1.2	0.0574	1.000	0.2287	0.840	0.6461	0.769	0.7884	0.710
1.4	0.0184	1.000	0.1746	0.815	0.6009	0.753	0.7552	0.697
1.6	0.0076	0.999	0.1282	0.790	0.5531	0.739	0.7204	0.688
1.8	0.0026	0.999	0.0902	0.766	0.5034	0.727	0.6841	0.683
2.0	0.0007	0.999	0.0606	0.742	0.4521	0.716	0.6458	0.680
2.2	0.0001	0.999	0.0387	0.720	0.4001	0.706	0.6054	0.679
2.4	0.0000	0.999	0.0234	0.699	0.3482	0.697	0.5627	0.679
2.6	0.0000	0.998	0.0133	0.680	0.2974	0.688	0.5174	0.679
2.8	0.0000	0.998	0.0071	0.662	0.2487	0.679	0.4694	0.680
3.0	0.0000	0.997	0.0035	0.646	0.2031	0.671	0.4186	0.680
3.2	0.0000	0.996	0.0016	0.631	0.1615	0.662	0.3648	0.681
3.6							0.2608	0.680
4.0							0.1708	0.677
4.4							0.1054	0.671
4.8							0.0627	0.663
5.2							0.0334	0.654
5.6							0.0156	0.640
6.0							0.0077	0.624
6.4							0.0040	0.613
6.8							0.0018	0.600
7.2							0.0009	0.586

Table 17. γ factor variation with observed transmittance for a 3LSRS ($D_1:D_2:D_3 = 1:1:1$; $T_1:T_2:T_3 = 30:10:3$) and Lorentzian-broadened absorber

$\Delta\nu_D$ (Source) / $\Delta\nu_N$ (Absorber)	0.1		1.0		3.0		10.0	
lnF	T	γ	T	γ	T	γ	T	γ
-3.2	0.9606	1.000	0.9782	0.998	0.9926	0.995	0.9983	0.992
-2.4	0.9143	1.000	0.9522	0.995	0.9836	0.989	0.9963	0.983
-1.6	0.8193	1.000	0.8972	0.989	0.9643	0.976	0.9920	0.964
-0.8	0.6417	1.000	0.7877	0.977	0.9243	0.949	0.9829	0.926
0.0	0.3726	1.000	0.5960	0.948	0.8471	0.899	0.9650	0.861
0.4	0.2293	1.000	0.4702	0.924	0.7889	0.865	0.9512	0.820
0.8	0.1111	1.000	0.3367	0.889	0.7162	0.826	0.9332	0.781
1.2	0.0377	1.000	0.2129	0.843	0.6297	0.787	0.9101	0.750
1.4	0.0183	1.000	0.1603	0.817	0.5819	0.767	0.8963	0.739
1.6	0.0076	1.000	0.1158	0.790	0.5318	0.752	0.8808	0.731
1.8	0.0026	1.000	0.0801	0.762	0.4800	0.737	0.8634	0.726
2.0	0.0007	0.999	0.0528	0.735	0.4272	0.723	0.8438	0.722
2.2	0.0001	0.999	0.0332	0.709	0.3742	0.710	0.8219	0.719
2.4	0.0000	0.999	0.0197	0.686	0.3222	0.697	0.7973	0.717
2.6	0.0000	0.999	0.0111	0.665	0.2720	0.684	0.7700	0.715
2.8	0.0000	0.998	0.0058	0.647	0.2247	0.672	0.7396	0.713
3.0	0.0000	0.998	0.0029	0.630	0.1812	0.661	0.7062	0.710
3.2	0.0000	0.997	0.0013	0.616	0.1424	0.649	0.6697	0.706
3.6							0.5878	0.697
4.0							0.4958	0.686
4.4							0.3977	0.673
4.8							0.2997	0.658
5.2							0.2091	0.642
5.6							0.1326	0.626
6.0							0.0750	0.610
6.4							0.0368	0.595
6.8							0.0153	0.581
7.2							0.0051	0.568

absorption experiments. Typically, in such experiments very reliable information about the source and absorber lineshapes is not available. The experimentalist may know whether the absorber lineshape is predominantly Gaussian or Lorentzian or whether the source is strongly self-reversed or not, and perhaps have an approximate idea of the source/absorber linewidth ratio involved. When only limited lineshape information is available, it is not profitable to perform exact calculations but the γ factor/observed absorption results given in Figs. 1–9 and Tables 1–20 may be scanned to find a source/absorber combination which approximates a given experimental situation. This procedure should allow the experimentalist to determine whether γ is constant or sufficiently slowly varying, for the modified Beer's law to be used.

Line-broadening in the absorber is the most important factor determining the behaviour of γ and not the occurrence of self-reversal in the source. Except for source linewidths which are

Table 18. γ factor variation with observed transmittance for a 3LSRS ($D_1:D_2:D_3 = 10:1:10$; $T_1:T_2:T_3 = 15:10:3$) and Lorentzian-broadened absorber

$\frac{\Delta\nu_D\ (\text{Source})}{\Delta\nu_N\ (\text{Absorber})}$	0.1		1.0		3.0		10.0	
lnF	T	γ	T	γ	T	γ	T	γ
-3.2	0.9611	1.000	0.9871	0.999	0.9978	0.999	0.9998	1.000
-2.4	0.9154	1.000	0.9715	0.998	0.9950	0.999	0.9995	1.000
-1.6	0.8215	1.000	0.9378	0.995	0.9890	0.998	0.9989	1.000
-0.8	0.6455	1.000	0.8675	0.988	0.9758	0.995	0.9976	0.999
0.0	0.3776	1.000	0.7319	0.974	0.9472	0.988	0.9947	0.998
0.4	0.2339	1.000	0.6311	0.961	0.9226	0.983	0.9921	0.998
0.8	0.1145	1.000	0.5092	0.944	0.8875	0.975	0.9883	0.997
1.2	0.0394	1.000	0.3744	0.920	0.8386	0.964	0.9826	0.995
1.4	0.0193	0.999	0.3070	0.905	0.8078	0.958	0.9788	0.994
1.6	0.0081	0.999	0.2428	0.889	0.7722	0.950	0.9741	0.993
1.8	0.0028	0.999	0.1844	0.871	0.7315	0.941	0.9686	0.991
2.0	0.0008	0.999	0.1337	0.851	0.6857	0.930	0.9618	0.989
2.2	0.0002	0.999	0.0920	0.830	0.6347	0.919	0.9536	0.987
2.4	0.0000	0.998	0.0598	0.809	0.5742	0.906	0.9438	0.984
2.6	0.0000	0.998	0.0365	0.788	0.5196	0.891	0.9320	0.982
2.8	0.0000	0.997	0.0207	0.767	0.4573	0.876	0.9179	0.978
3.0	0.0000	0.996	0.0104	0.746	0.3937	0.859	0.9010	0.974
3.2	0.0000	0.995	0.0053	0.727	0.3305	0.842	0.8810	0.969

Table 19. γ factor variation with observed transmittance for a 3LSRS ($D_1:D_2:D_3 = 100:1:100$; $T_1:T_2:T_3 = 15:10:3$) and Lorentzian-broadened absorber

$\frac{\Delta\nu_D\ (\text{Source})}{\Delta\nu_N\ (\text{Absorber})}$	0.1		0.5		1.0		3.0	
lnF	T	γ	T	γ	T	γ	T	γ
-3.2	0.9617	1.000	0.9795	0.999	0.9912	0.999	0.9987	1.000
-2.4	0.9167	1.000	0.9549	0.999	0.9804	0.998	0.9971	1.000
-1.6	0.8240	1.000	0.9026	0.997	0.9571	0.996	0.9936	0.999
-0.8	0.6500	1.000	0.7967	0.993	0.9074	0.992	0.9859	0.998
0.0	0.3834	1.000	0.6053	0.985	0.8070	0.982	0.9689	0.995
0.4	0.2393	1.000	0.4753	0.977	0.7280	0.974	0.9541	0.993
0.8	0.1185	1.000	0.3334	0.966	0.6262	0.962	0.9325	0.990
1.2	0.0415	0.999	0.1991	0.950	0.5032	0.945	0.9014	0.985
1.4	0.0205	0.999	0.1420	0.940	0.4362	0.935	0.8813	0.982
1.6	0.0087	0.998	0.0949	0.928	0.3678	0.922	0.8574	0.978
1.8	0.0030	0.999	0.0587	0.914	0.3004	0.909	0.8294	0.974
2.0	0.0008	0.998	0.0332	0.899	0.2363	0.894	0.7967	0.968
2.2	0.0002	0.998	0.0170	0.883	0.1782	0.878	0.7590	0.962
2.4	0.0000	0.997	0.0077	0.866	0.1279	0.862	0.7158	0.954
2.6	0.0000	0.997	0.0031	0.849	0.0869	0.846	0.6673	0.945
2.8	0.0000	0.996	0.0011	0.833	0.0554	0.830	0.6134	0.935
3.0	0.0000	0.995	0.0003	0.812	0.0328	0.815	0.5547	0.924
3.2	0.0000	0.993	0.0001	0.791	0.0179	0.801	0.4922	0.911

Table 20. γ factor variation with observed transmittance for a 3LSRS ($D_1:D_2:D_3 = 1:1:1$; $T_1:T_2:T_3 = 15:10:3$) and Voigt-broadened absorber with Lorentzian width/Gaussian width = 1

$\frac{\Delta\nu_D\ (\text{Source})}{\Delta\nu_D\ (\text{Absorber})}$	0.1		1.0		3.0		10.0	
lnF	T	γ	T	γ	T	γ	T	γ
-3.2	0.9602	1.000	0.9710	0.999	0.9889	0.994	0.9974	0.991
-2.4	0.9136	1.000	0.9367	0.997	0.9756	0.988	0.9943	0.979
-1.6	0.1879	1.000	0.8650	0.994	0.9473	0.973	0.9876	0.955
-0.8	0.6392	1.000	0.7256	0.987	0.8896	0.942	0.9739	0.907
0.0	0.3694	1.000	0.4949	0.969	0.7830	0.881	0.9481	0.822
0.4	0.2264	1.000	0.3552	0.953	0.7072	0.837	0.9290	0.768
0.8	0.1090	1.000	0.2205	0.926	0.6177	0.785	0.9052	0.716
1.2	0.0367	1.000	0.1129	0.884	0.5189	0.734	0.8753	0.676
1.4	0.0176	1.000	0.0740	0.855	0.4678	0.711	0.8598	0.663
1.6	0.0072	1.000	0.0455	0.821	0.4165	0.691	0.8415	0.655
1.8	0.0024	1.000	0.0262	0.783	0.3658	0.674	0.8214	0.652
2.0	0.0006	1.000	0.0142	0.741	0.3164	0.660	0.7992	0.652
2.2	0.0001	1.000	0.0072	0.699	0.2690	0.648	0.7747	0.653
2.4	0.0000	1.000	0.0034	0.661	0.2243	0.639	0.7476	0.656
2.6	0.0000	1.000	0.0015	0.628	0.1830	0.630	0.7177	0.659
2.8	0.0000	1.000	0.0006	0.600	0.1457	0.623	0.6849	0.662
3.0	0.0000	1.000	0.0003	0.577	0.1128	0.616	0.6492	0.664
3.2	0.0000	1.000	0.0001	0.559	0.0848	0.610	0.6106	0.665

significantly narrower than the absorber linewidth (when γ approaches unity), Doppler-broadened absorbers never exhibit γ factors which are sufficiently slowly varying for the modified Beer's law to be used. Substantial line-wing absorption appears to be essential for γ to become slowly varying or nearly constant. With absorbers which are Lorentzian-broadened, or Voigt-broadened with significant Lorentzian character, γ sometimes becomes relatively slowly varying for linewidth ratios ~3 and nearly constant for linewidth ratios ~10. Linewidth ratios as large as the latter are very unlikely to be encountered in practice. We conclude that, even

with a Lorentzian or Voigt-broadened absorber, γ factors greatly different from unity and slowly varying with absorption should not occur. It must be admitted that many real experimental situations are more complex than the source/absorber models we have used and other factors not considered in our models may contrive to make γ a slowly varying factor under some conditions. However, in general, we feel that data obtained in time-resolved atomic absorption experiments analyzed with γ factors greatly different from unity, say <0.9, should be viewed with suspicion unless data demonstrating that $\ln\ln(I_0/I)$ vs ln (absorber concentration) plots are linear throughout the range of absorber concentrations used in the analysis, are presented. Once γ is recognized as a varying function of absorption, attention can then be paid to whether an average value of γ, appropriate to the range of absorptions observed in the experiment, should be used to give more accurate results than would be obtained by assuming that $\gamma = 1$. For example, in Fig. 3, which treats a Doppler-broadened source and Lorentzian absorber, for observations made between 0 and 40% absorption, with a source/absorber linewidth ratio = 3, γ varies from 1 to 0.78. It would probably be more reliable in such a situation to use an average value of γ, 0.89 and treat this as constant, rather than neglect γ entirely and use $\gamma = 1$.

It should be noted that inaccuracies introduced because γ is not constant and not equal to unity are not in general increased by using self-reversed sources. Consequently, in atomic absorption experiments it is better to try and make the source/absorber linewidth less than unity rather than expend effort in avoiding self-reversal in the source.

One further complication in time-resolved atomic absorption experiments is that the lineshape of the absorber may in theory itself be time-dependent, although hopefully this should not happen in practice, particularly when the absorber is present in a large excess of diluent. If this lineshape were to vary, its time-dependence would probably be unknown and any attempt at reliable analysis of the data would be impossible. Indeed, one could conceive of a situation where the time-dependence of the absorber lineshape were such as to produce observed absorptions apparently satisfying eqn (16), with a constant γ, but in fact yielding totally erroneous values of τ. It would therefore appear important to ascertain that the absorber lineshape is not time-dependent through being a function of absorber concentration. Without this possible complication, in measurements of the decay rate of transient absorbers where the modified Beer's law is not approximately correct, it follows from eqn (13) after writing $F = F_0 e^{-t/\tau}$ that

$$T = 1 - aF_0 e^{-t/\tau} + \frac{bF_0^2 e^{-2t/\tau}}{2!} - \frac{cF_0^3 e^{-3t/\tau}}{3!} + \cdots, \tag{37}$$

if measurements are made for small values of F, direct numerical fitting of a function containing a few terms of eqn (37) should yield accurate values for τ, without using an unreal γ factor to analyze the data as in eqn (16).

Acknowledgements—Support for this research was obtained from the National Science Foundation through the Materials Science Center, Cornell University and from the Air Force Office of Scientific Research (AFSC) under Grant 75-2781. Discussions with D. H. BURDE on his kinetics studies using absorption spectroscopy are gratefully acknowledged.

REFERENCES

1. A. C. G. MITCHELL and M. W. ZEMANSKY, *Resonance Radiation and Excited Atoms*. Cambridge University Press, London (1971).
2. G. V. MARR, *Plasma Spectroscopy*. Elsevier, Amsterdam (1968).
3. M. ABRAMOWITZ and I. A. STEGUN, *Handbook of Mathematical Functions*. Dover, New York (1968).
4. V. N. FADEEVA and N. M. TERENT'EV, *Tables of Values of the Probability Integral for Complex Arguments*. State Publishing House for Technical Literature, Moscow (1954).
5. B. D. FRIED and S. D. CONTE, *The Plasma Dispersion Function*. Academic, New York (1961).
6. J. V. V. KASPER and G. C. PIMENTEL, *Appl. Phys. Lett.* **5**, 231 (1964).
7. R. J. PIRKLE, J. R. WIESENFELD, C. C. DAVIS, G. J. WOLGA and R. A. MCFARLANE, *IEEE J. Quant. Electron* **QE-11**, 834 (1975).
8. T. W. HANSCH, *Appl. Opt.* **11**, 895 (1972).
9. H. PRUGGER, *Optik* **21**, 320 (1964).
10. F. A. MORSE and F. KAUFMAN, *J. Chem. Phys.* **42**, 1785 (1965).
11. D. A. PARKES, L. F. KEYSER and F. KAUFMAN, *Astrophys. J.* **149**, 217 (1967).
12. F. KAUFMAN and D. A. PARKES, *Trans. Faraday Soc.* **66**, 1579 (1970).

13. W. Braun and T. Carrington, *JQSRT* **9**, 1133 (1969).
14. A. B. Prag, C. E. Fairchild and K. C. Clark, *Phys. Rev.* **A137**, 1358 (1965).
15. J. V. Michael and R. E. Weston, Jr., *J. Chem. Phys.* **45**, 3632 (1966).
16. P. B. Bemand and M. A. A. Clyne, *Chem. Soc. Faraday Trans. II* **69**, 1643 (1973).
17. H. J. Kostkowski and A. M. Bass, *J. Opt. Soc. Am.* **46**, 1060 (1956).
18. R. J. Donovan, D. Husain and L. J. Kirsch, *Trans. Faraday Soc.* **66**, 2551 (1970).
19. R. J. Donovan, D. Husain and L. J. Kirsch, *Trans. Faraday Soc.* **67**, 375 (1971).
20. J. J. Deakin, D. Husain and J. R. Wiesenfeld, *Chem. Phys. Lett.* **10**, 146 (1971).
21. R. F. Heidner II, D. Husain and J. R. Wiesenfeld, *Chem. Phys. Lett.* **16**, 530 (1972).
22. M. J. Bevan and D. Husain, *J. Photochem.* **3**, 1 (1974).
23. A. Brown and D. Husain, *J. Photochem.* **3**, 37 (1974).
24. A. Brown and D. Husain, *J. Less-Common Metals* **3**, 305 (1974).
25. D. H. Burde, R. A. McFarlane and J. R. Wiesenfeld, *Phys. Rev.* **A10**, 1917 (1974).
26. M. J. Bevan and D. Husain, *J. Photochem.* **4**, 51 (1975).
27. D. H. Burde, R. A. McFarlane and J. R. Wiesenfeld, *Chem. Phys. Lett.* **32**, 296 (1975).
28. A. Reichel, *JQSRT* **8**, 1601 (1968).
29. E. E. Whiting, *JQSRT* **8**, 1379 (1968).
30. K. G. Harstad, *J. Opt. Soc. Am.* **62**, 827 (1972).
31. T. Donohue and J. R. Wiesenfeld, *J. Chem. Phys.* **63**, 3130 (1975).
32. C. C. Davis and R. A. McFarlane, Laboratory of Plasma Studies Report No. 182, Cornell University, Jan. 1976.

APPENDIX

For the source/absorber models we have considered, it has been assumed that the absorber concentration is uniform along the absorption path, and further, that all rays from the source which eventually reach the detection system travel along paths of the same length through the absorber. Under these conditions, the following relationship holds:

$$I/I_0 = 1 - aF + \frac{bF^2}{2!} - \frac{cF^3}{3!} + \cdots, \tag{38}$$

where $F = kNL\sigma$, and $a, b, c, \ldots$ are constants determined by the lineshapes of source and absorber. We can show that a similar relation still holds even if the absorber concentration is spatially non-uniform and the detection system receives rays which have travelled along paths of different length through the absorbing material. We will, however, assume that all these rays do come from regions of the source which have the same lineshape.

Under these conditions, pencils of radiation labelled i travel from different areas of the source along various optical paths through the absorber to the detection system. For each pencil i, assumed to consist of a fine bundle of parallel rays travelling along the same path from source to absorber, the absorption coefficient experienced at some point z_i along its path is

$$\alpha_i(\nu, z_i) = kN_i(z_i)g(\nu), \tag{39}$$

where $N_i(z_i)$ is the concentration of absorbers at point z_i, k is a constant and $g(\nu)$ is the lineshape function of the absorber (assumed to be independent of position within the absorber).

If the intensity of the ith pencil at frequency ν is $I_i(\nu, z_i)$, then

$$\alpha_i(\nu, z_i) = \frac{-1}{I_i(\nu, z_i)} \frac{\mathrm{d}I_i(\nu, z_i)}{\mathrm{d}z_i}, \tag{40}$$

which, in view of eqn (39), gives

$$I_i(\nu, z_i) = I_0 g_s(\nu) \exp\left[-\int_{L_i} kN_i(z_i)g(\nu)\,\mathrm{d}z_i\right]. \tag{41}$$

where the integral is taken along the path of the ith pencil, L_i. I_0 is the initial total intensity in the pencil as it enters the absorber and $g_s(\nu)$ is the source lineshape. For many such pencils,

$$\sum_i I_i(\nu, z_i) = g_s(\nu) \sum_i I_{0_i} \exp\left[-\int_{L_i} kN_i(z_i)g(\nu)\,\mathrm{d}z_i\right] \tag{42}$$

and the total observed intensity is

$$I = \sum_i \int_{-\infty}^{\infty} I_0 g_s(\nu) \exp\left[-\int_{L_i} kN_i(z_i)g(\nu)\,\mathrm{d}z_i\right]. \tag{43}$$

We can write $\int_{L_i} N_i(z_i)\,\mathrm{d}z_i = k\bar{N}_i l_i$, where $\bar{N}_i$ is the average value of N_i over absorption path i of length l_i. Thus,

$$I = \sum_i \int_{-\infty}^{\infty} I_0 g_s(\nu) \left\{1 - k\bar{N}_i l_i g(\nu) + \frac{(k\bar{N}_i l_i)^2}{2!}[g(\nu)]^2 - \cdots\right\} \mathrm{d}\nu, \tag{44}$$

$$= I_0 - ka' \sum_i I_{0_i} \bar{N}_i l_i + \frac{k^2 b'}{2!} \sum_i I_{0_i} (\bar{N}_i)^2 l_i^2 - \cdots \tag{45}$$

where I_0 is the total intensity of the radiation in the absence of absorbers and

$$a' = \int_{-\infty}^{\infty} g_s(\nu)g(\nu)\,d\nu, \qquad b' = \int_{-\infty}^{\infty} g_s(\nu)[g(\nu)]^2\,d\nu, \ldots$$

We can write the intensity of the ith pencil as $I_{0_i} = p_i I_0$, where p_i is a factor determined by the geometry of the experiment. Similarly, for the average concentration of absorbers along the path of the ith pencil we write $\bar{N}_i = q_i\bar{N}$, where $\bar{N}$ is the total average concentration of absorbers and q_i is another geometrical factor. The length of the ith pencil we write as $l_i = r_i L$, where L is the length of the absorption cell. Thus, eqn (45) becomes

$$I/I_0 = 1 - a'k\bar{N}L\sum_i p_i q_i r_i + \frac{b'[k\bar{N}L]^2}{2!}\sum_i p_i q_i^2 r_i^2 - \cdots, \tag{46}$$

$$= 1 - AF + \frac{BF^2}{2!} - \frac{CF^3}{3!} + \cdots, \tag{47}$$

where $F = k\bar{N}L\sigma$, a result similar to eqn (38) but where the new constants A, B, C, ... are determined by geometrical factors as well as by the line-shape functions of source and absorber, i.e.

$$A = \frac{a'}{\sigma}\sum_i p_i q_i r_i, \qquad B = \frac{b'}{\sigma^2}\sum_i p_i q_i^2 r_i^2 \ldots.$$

If we do not assume that radiation coming from all parts of the source has the same line-shape, then eqn (44) becomes

$$I = \sum_i \int_{-\infty}^{\infty} I_{0_i} g_{s_i}(\nu)\left\{1 - k\bar{N}_i l_i g(\nu) + \frac{[k\bar{N}_i l_i]^2}{2!} - \cdots\right\} d\nu, \tag{48}$$

where $g_{s_i}(\nu)$ is the line-shape function of the source emission which constitutes the ith pencil. Thus,

$$I = I_0 - k\sum_i a_i' I_{0_i}\bar{N}_i l_i + \frac{k^2}{2!}\sum_i b_i' I_{0_i}\bar{N}_i^2 l_i^2 - \cdots, \tag{49}$$

where $a_i' = \int_{-\infty}^{\infty} g_{s_i}(\nu)g(\nu)\,d\nu$, $b_i' = \int_{-\infty}^{\infty} g_{s_i}(\nu)[g(\nu)]^2\,d\nu \ldots$ and

$$I/I_0 = 1 - AF + \frac{BF^2}{2!} - \frac{CF^3}{3!} + \cdots, \tag{50}$$

where $A = \frac{1}{\sigma}\sum_i a_i' p_i q_i r_i$, $B = \frac{1}{\sigma^2}\sum_i b_i' p_i q_i^2 r_i^2 \ldots$. If all pencils have the same intensity, that is if the source has uniform radiance, then $p_i = 1/n$ where n is the total number of pencils altogether. Further, if all paths through the absorber contain the same uniform concentration of absorbers, then $q_i = 1$ and, if all paths are the same length, $r_i = 1$. Even if the line-shape function of the absorbers is not independent of position, which is an extremely unlikely occurrence, an equation of the form of eqn (50) still holds but simple analytic expressions for the value of the constants A, B, C, ... in terms of geometric factors and line-shape functions do not exist.

Temperature Dependence of the Collisional Deactivation of Excited Iodine Atoms $I(5p^5\ ^2P_{1/2})$

D. H. Burde

Department of Applied Physics
Cornell University
Ithaca, New York 14853*

and

R. A. McFarlane

School of Electrical Engineering
and Matericals Science Center
Cornell University
Ithaca, New York 14853

Support for this research was obtained from the Materials Science Center, Cornell University and from the Air Force Office of Scientific Research (AFSC) under Grant #75-2781.

*Currently with Aeronautical Research Associates of Princeton, Inc., Princeton, NJ 08540.

Abstract

The collisional deactivation of excited iodine atoms $I(5p^5\ ^2P_{1/2})$ by I_2, O_2, H_2, HD, and D_2 has been studied as a function of temperature from 295° k to 600° k. The decay of the excited iodine atom concentration following dye laser photolysis of molecular I_2 was detected by time-resolved atomic absorption (295° k) and by time-resolved atomic fluorescence at 1.315 μm. The advantages and disadvantages of the two techniques are considered and the experimental results are compared to an earlier study. Very substantial discrepancies in the temperature dependence of quenching by molecular I_2 are observed when the present results are compared with previous measurements.

I. Introduction

The collisional deactivation of electronically excited iodine atoms $I^*(5p^5\ ^2P_{1/2})$ has been the subject of many experimental[1-3] and theoretical[4-6] investigations. The majority of the experimental work has employed the technique of time-resolved atomic absorption to monitor the I* concentration. These studies have generally employed high energy flashlamps to flash photolyze I_2 or iodine compounds to produce I* atoms. In a new technique developed in this laboratory, a tunable dye laser was used instead of a broadband flashlamp system[7] to selectively photolyze I_2. Combined with time-resolved absorption, the excited atom concentration could be monitored on a very much shorter timescale than was previously possible. The excellent time response and sensitivity of the system were utilized to investigate the collisional production of I* atom from excited I_2 molecules[7,8] and to measure the quenching rate of I* by several gases at room temperature.[9,10]

The present paper reports the rates of quenching of I* atoms by I_2, O_2, H_2, HD, and D_2 over a wide temperature range. The quenching rates were first determined at room temperature using time-resolved absorption. Then, the quenching rates were determined between room temperature and 300° C using time-resolved fluorescence from I* atoms at 1.315 μ. The advantages and disadvantages of the two techniques are considered. The validity of the modified Beer-Lambert law used extensively in analysis of time-resolved absorption experiments is discussed in detail. Finally, the experimental results are compared

to an earlier study[11] of the temperature dependence of I* quenching which employed the absorption technique exclusively. Very substantial discrepancies are observed in the case of quenching by molecular iodine.

II. Time-Resolved Atomic Absorption: Room Temperature Data

A. Relation Between Observed Absorption Signals and Absorber Concentration

In absorption experiments, the observed absorption signal must be related to the absorber concentration in order to extract useful kinetic data. In general, the relation between absorption and absorber concentration is complicated and approximations are usually made. In particular, the modified Beer-Lambert law $I_{tr} = I_o \exp[-(\varepsilon N \ell)^{\gamma}]$ describing the light intensity transmitted through an absorbing sample has appeared extensively in the literature in the analysis of time-resolved absorption experiments. There has been some confusion as to the limits of validity of this approximation and the physical meaning of "γ factors". This section will discuss these considerations.

Let $I(\nu_R)$ be the intensity of a monochromatic wave of frequency ν_R propagating in a homogeneous medium. Let N_2 denote the concentration of species in the upper state of the transition involved and N_1 denote the concentration of species in the lower state. As the wave propagates, the variation in the intensity due to induced transition is given by[12-14]

$$\frac{dI(\nu_R, z)}{dz} = -\left\{ \left[N_1 \frac{g_2}{g_1} - N_2 \right] \frac{c^2 A_{21}}{8\pi\nu_R^2} \, g(\nu_R) \right\} I(\nu_R, z) \qquad (1)$$

where $g(\nu)$ = the normalized absorption lineshape function for the transition. Therefore, the intensity varies with distance as

$$I(\nu_R, z) = I(\nu_R, 0)\, e^{-\alpha(\nu_R)z}. \tag{2}$$

For most experiments employing absorption techniques, $N_2 \ll N_1\, g_2/g_1$ and therefore

$$\alpha(\nu_R) = \frac{c^2 A_{21} g_2}{8\pi \nu_R^2\, g_1}\; g(\nu_R) N \tag{3}$$

where $N \equiv N_1$. The atomic (or molecular) absorption coefficient at frequency ν_R is given by

$$\varepsilon(\nu_R) = \varepsilon_L\, g(\nu_R) \tag{4}$$

$$\text{where } \varepsilon_L = \frac{c^2 A_{21} g_2}{8\pi \nu_o^2\, g_1}. \tag{5}$$

Here ν_R has been (very closely) approximated by ν_o, the line center transition frequency because only for values of ν_R very close to ν_o is $g(\nu_R)$ non-zero.

Finally, the intensity after path length ℓ is

$$I(\nu_R, \ell) = I(\nu_R, 0) e^{-\varepsilon(\nu_R) N \ell}. \tag{6}$$

This is the Beer-Lambert law for a monochromatic wave. The absorber concentration N may, of course, be a function of time.

In general, the radiation entering the absorbing medium (as from a resonance lamp) is not monochromatic but rather has a finite bandwidth which can be described by a normalized lineshape function $p(\nu)$. In this case, an integration over frequency is necessary and gives

$$I(\ell) = I(o)\int_{-\infty}^{\infty} p(\nu)e^{-\varepsilon_L N\ell g(\nu)}d\nu. \qquad (7)$$

Therefore, unless the absorption lineshape function $g(\nu)$ is constant over the range of frequencies in the emission line, a simple Beer-Lambert law will not accurately describe the intensity variation. Usually, the detailed lineshapes $g(\nu)$ and $p(\nu)$ are not known and may be very complicated. What is needed is a relation which is analytically tractable and approximately correct over a limited range of absorption. A modified Beer-Lambert law of the form

$$I_{tr}(\ell) = I(o)\ e^{-(\varepsilon N\ell)^{\gamma}} \qquad (8)$$

has been proposed.[15] In this relation, I_{tr} is the light intensity transmitted through an absorption cell of length ℓ and $I(o)$ is the intensity of the transmitted light when $N = 0$. γ is an empirical parameter, $\gamma \leq 1$, which must be determined experimentally. For a γ factor of 1, this law reduces to the simple Beer-Lambert law. However, γ values much less than 1 indicate a significant deviation from the simple law. In that case, this approximate law will generally only be useful over a limited range of absorption. It should be

noted here that, unfortunately, in much of the earlier work this law was written as $I_{tr} = I(o)\exp[-\varepsilon(N\ell)^{\gamma}]$, resulting in units of $(N\ell)^{-\gamma}$ for ε. To be correct dimensionally, Eqn. (8) must be used. In either case, the kinetic analysis of the experimental results depends only on the fact that the concentration N appears to the power γ. Therefore, both forms yield the same results.

The utility of the modified Beer-Lambert law for time dependent kinetic studies is immediately obvious by observing that $\ln[I(o)/I(t)] = (\varepsilon N(t)\ell)^{\gamma} = \text{const} \times (N(t))^{\gamma}$. As the overwhelming majority of the time-resolved experiments involve monitoring a simple exponential decay of the absorber concentration, $N(t) = N(0_+) \exp(-kt)$, the observed time dependence is therefore described by $(N(t))^{\gamma} \alpha \exp(-k\gamma t)$, again a simple exponential decay but with an observed decay rate of $k_{oBS} = k\gamma$. Thus, use of an approximate law of this form simplifies analysis of kinetic data.

The validity of this modified Beer-Lambert law has been studied in detail.[16] Transmission integrals for a variety of emission and absorption lineshapes were numerically integrated and γ values were determined as a function of percent absorption. As expected, γ values were not strictly constant over a wide range of absorptions. However, for absorptions of less that 15%, γ values in the range 0.8 to 1.0 gave good approximations to the theoretical calculations for a wide variety of lineshapes. The calculations show that as absorption $\to 0$, $\gamma \to 1$ regardless of lineshapes.

A gamma factor can be found experimentally where absorbers are produced by a photolysis pulse at t = 0 by plotting $\ln\{\ln[I_{tr}(t=0)/I_{tr}(t=0_+)]\}$

versus ln $N(t = 0_+)$. This yields a straight line of slope γ if this modified law is valid. A curvature in the plot would indicate that γ is not a constant over that particular range of absorptions. For many experimental conditions, γ has been found to remain nearly constant over a reasonable range of absorptions and this modified Beer-Lambert law has proved to be a useful approximation.

For the experimental arrangement used in the present study, γ was found to be 0.89 ± 0.07 for absorptions of up to 15%.[9] This is in good agreement with the theoretical calculations and only a minor correction to the simple Beer-Lambert law is necessary. This is one significant advantage of the present experiment which involved only small absorptions over earlier studies in which absorptions greater than 50% were typical. For small absorptions, the effects of complex lineshapes are minimized, "γ factors" are close to 1, and the simple Beer-Lambert law is nearly correct. Although the signal-to-noise ratio is relatively poor for a single shot, the signal averaging technique very effectively improves this to acceptable levels. Computer fits utilizing a few hundred points per average absorption trace can give decay rates accurate to a few percent.

B. Experimental

A block diagram of the experimental apparatus is shown in Figure 1. A nitrogen laser was used to pump a dye laser. The nitrogen laser produced a 10 nsec, 2 mJ pulses at 337.1 nm at a repetition rate of approximately 20 Hz. The dye laser produced 8 nsec pulses of 50-150 μJ with a bandwidth of roughly 0.1 Å, tunable from 470.0 nm to 525.0 nm

using 4-methylumbelliferone dye in an acidic methanol solution.

The dye laser pulses (or the N_2 laser pulses, in experiments with n - C_3F_7I) were admitted to an externally mirrored cell and underwent a multiple bounce path down the cell. Atomic iodine resonance radiation produced by a microwave powered iodine lamp passed through the cell and into a McPherson Model 225 vacuum ultraviolet monochromator which was used to isolate the 206.2 nm line corresponding to the transition $I(6s\ ^2P_{3/2}) \leftarrow I(5p^5\ ^2P_{1/2})$. Absorption at this wavelength permitted the observation of the excited atom $I^*(5p^5\ ^2P_{1/2})$ concentration as a function of time following each laser pulse. The absorption signal was monitored by a Hamamatsu type R106UH photomultiplier tube and was digitized by a Biomation Model 8100 transient recorder. Following each laser pulse, the waveform was digitally transferred to a Northern Scientific Model 575 signal averager. The time constant of the detection system was measured to be 20 nsec. Due to the relatively weak absorption and low single shot signal-to-noise ratio, typically 10^4 absorption traces were signal averaged. The data was the transferred to magnetic tape using a Texas Instruments Model 733ASR electronic data terminal. The data was then read into an IBM 370 computer and analyzed using non-linear least squares fitting routines.[12]

Pressure measurements of the gases in the absorption cell were made by two gauges attached directly to the cell. A very high precision capacitance manometer (MKS Baratron Type 305AH-10) was used to measure pressures up to 10 torr with a sensitivity of 10^{-4} torr. In addition, a monel bourdon tube type pressure sensor (Robinson-Halpern Model 144A)

was used to measure pressures up to 760 torr. The absorption cell was attached to a grease-free gas handling system evacuable to 10^{-6} torr.

Research grade O_2, H_2 (Linde), HD (Merck, Sharp, and Dohme), and D_2 (Air Products) were used directly. Individual batch analyses showed negligible impurity levels. Baker reagent grade I_2 was distilled onto P_2O_5 to remove water vapor and then fractionally distilled into the absorption cell. The n - C_3F_7I (PCR) was fractionally distilled twice from dry ice-methanol baths to remove impurities.

C. Room Temperature Data and Results

The rate of decay of excited iodine atoms following the photolyzing flash is given by

$$d[I^*]/dt = - (A_{nm} + k_D + \sum_Q k_Q[Q])\ [I^*] = -k[I^*]. \qquad (9)$$

The contribution to the overall decay by spontaneous emission, A_{nm}, and diffusion, k_D, were negligible. Under these conditions,

$$d[I^*]/dt = -(\sum_Q k_Q[Q])\ [I^*] = -k[I^*] \qquad (10)$$

which upon integration yields

$$[I^*(t)] = [I^*(o)] \exp(-kt) \qquad (11)$$

where the photolyzing flash occurs at t = 0. The terms of the form $k_Q[Q]$ represent quenching due to collisions between an excited iodine atom and a molecule of species Q.

The modified Beer-Lambert law $I_{tr}(t) = I(o) \exp[-(\varepsilon N(t)\ell)^{\gamma}]$ was used in the analysis where $N(t) = [I^*(t)]$ and $\gamma = 0.89$. For the small absorptions observed (< 10%), the exponential term may be accurately approximated by expanding in a Taylor's series keeping only first order terms to give

$$I_{tr}(t) = I(o) \{ 1 - (\varepsilon\ell)^{\gamma} [I^*(t)]^{\gamma} \} \text{ or} \qquad (12)$$

$$I_{tr}(t) = I(o) - \text{const} \times [I^*(t)]^{\gamma} \qquad (13)$$

where $[I^*(t)] = [I^*(o)] \exp(-kt)$ (Eqn. 11). The observed decay rate is therefore $k_{OBS} = \gamma k$ and $k = k_{OBS}/\gamma$. For each experimental run, k was calculated in this manner from k_{OBS}.

In the experiments with H_2 and D_2, n - C_3F_7I was used as the source material for I* atoms. The N_2 laser was used directly to photolyze n - C_3F_7I as this compound absorbs in the ultraviolet. For the studies employing HD, I_2 was photolyzed by the dye laser at 505.0 nm. The pressure of I_2 in the absorption cell was held constant by immersing a sidearm coldfinger containing excess I_2 crystal in a 0° C bath, yielding $P_{I_2} = 0.03$ torr, which was monitored using the capacitance manometer. All data were taken at room temperature.

The data for H_2, HD, and D_2 are plotted in Figures 2-4. The second order quenching rate constants at 295° k are summarized in

Table I. The results for I_2 and O_2 have been reported and discussed earlier.[9,10] Of particular interest here is the striking difference observed in quenching efficiency between H_2, HD, and D_2. In the work of Butcher et al.,[6] the relative rates $k_{HD} > k_{H_2} > k_{D_2}$ were explained in terms of resonant E → V + R exchange. Zimmerman and George carried out rigorous quantum mechanical calculations for collisions restricted to collinear configurations to yield transition probabilities between the spin-orbit states of the atom ($^2P_{1/2}$ and $^2P_{3/2}$) and vibrational states of the molecule. Their findings predict the same ordering of quenching efficiencies as Butcher et al. The present results confirm the earlier findings of these large isotope effects. The temperature dependence of these quenching rates can be useful in elucidating the details of the quenching mechanism.[5,6] This is discussed in the following section.

III. *Time-Resolved Fluorescence:* Temperature Dependence of the Quenching Rates

A. Experimental

The temperature dependence of the quenching rates for I_2, O_2, H_2, HD, and D_2 were investigated from room temperature to approximately 300° C. In order to eliminate the complication of a γ factor and its possible variation with temperature, these studies were carried out using the time-resolved fluorescence technique. A block diagram of this experimental setup is shown in Fig. 5. A cylindrical fluorescence cell was constructed of pyrex and wrapped with heating tape. Three thermocouples were placed along the cell to provide temperature measurements. A temperature controller was used to control the current applied to the heating tape and to thereby maintain the cell at selectable fixed temperatures. Fluorescence was observed at 90° to the photolyzing dye laser beam through a double window assembly, evacuated to provide thermal insulation. An InSb detector was used in conjunction with an infrared bandpass filter to detect 1.315 μ radiation corresponding to the transition

$$I^*(5p^5\ ^2P_{1/2}) \rightarrow I(5p^5\ ^2P_{3/2}) + h\nu(1.315\ \mu m). \qquad (14)$$

The observed fluorescence intensity is directly proportional to $[I^*(t)]$, greatly simplifying the analysis. Therefore, the observed fluorescence signals were of the form (Eqn. 11)

$$I_{fl}(t) = I(0)\ \exp(-kt). \qquad (15)$$

The A coefficient for this electric-dipole forbidden transition is very small[18-20] and hence this radiation is relatively weak. Significantly greater concentrations of excited atoms were required for acceptable signals in this system as compared to the absorption system. For this reason, a higher energy flashlamp-pumped dye laser (Phase-R DL2100C) was used to flash photolyze molecular I_2 to produce I* atoms. The laser was run untuned with coumarin 102 and produced 300 nsec, 50-150 mJ pulses centered near 480 nm to promote I_2 molecules into the B state continuum and produce I* atoms by photodissociation.[7] The remainder of the system was identical to that shown in Fig. 1. The response time of the fluorescence detection system was limited by the InSb detector and was approximately 1 μsec. The use of molecular I_2 as the photolyzed material rather than an iodine compound eliminated the possibility of contributions to the observed decay by any radicals produced during photolysis. These radicals may have significantly affected earlier high-power flashlamp photolysis studies.

B. Data Analysis and Results

$\underline{I_2}$

The first experiments were carried out with pure I_2 in the fluorescence cell. In order to confirm our previously reported value of k_{I_2} at room temperature obtained by the atomic absorption technique,[9] a series of runs were carried out at different I_2 pressures as controlled by a sidearm coldfinger attached to the fluorescence cell. The data is plotted in Fig. 6. The value $k_{I_2} = 3.7 \pm 0.3 \times 10^{-11}$ cm^3 molecule^{-1} sec^{-1} was obtained, in excellent agreement with our previous result which also has been confirmed by other workers.[21-23]

In the work of Deakin and Husain who studied the temperature dependence of k_{I_2} employing time-resolved absorption,[11] a series of runs were also taken at room temperature and a value of $k_{I_2} = 4.1 \times 10^{-12}$ cm^3 $molecule^{-1}$ sec^{-1} was obtained, a very serious discrepancy. In their experiment, no coldfinger containing excess I_2 crystal was directly connected to the reaction vessel. Rather, helium, used as a buffer gas, was circulated through a glass spiral containing I_2 crystals held at various slush temperatures and then into the reaction vessel. It was assumed that the (partial) pressure of I_2 was equal everywhere in the system to its vapor pressure at the slush temperature. The reaction vessel was then sealed off and an experimental run taken. It is possible that incomplete mixing resulted in a pressure of I_2 in the reaction vessel of less than that expected, resulting in a slower observed decay and therefore in a much smaller indicated value of k_{I_2}. There may also have been an additional drop in I_2 pressure once the reaction vessel was sealed off. In our own work using the high precision capacitance manometer, it has been clearly seen that if I_2 vapor is admitted to a cell without excess crystal in a coldfinger and the cell is scaled off with a greaseless teflon stepcock, the pressure invariably falls. This effect is also evident visually as a brown staining of the teflon. Therefore, in all experiments requiring a fixed pressure of I_2 vapor, it is recommended that a coldfinger with excess I_2 crystal be attached to the cell.

For all of the present temperature dependent studies, a coldfinger containing I_2 crystals attached to the fluorescence cell was immersed in a 0° C bath. The coldfinger tube diameter was greater

than ten times the mean free path of I_2 molecules and therefore thermal transpiration effects between the coldfinger and the heated section of the fluorescence cell were negligible. The degree of thermal dissociation of I_2 vapor was also considered. Several workers[24-27] have studied the dissociation process $I_2(g) \rightleftarrows 2I(g)$. The equilibrium constant for this process, $K_p = (P_I)^2/P_{I_2}$ (pressure measured in atmospheres), is related to the change in the free energy by $\ln K_p = -\Delta F°/RT$. Using the latest thermochemical data for the free energy of $I_2(g)$ and $I(g)$,[28] K_p was calculated from this relation yielding values in very good agreement with the experimental data. At the highest temperature reached in the present studies, T = 643° K, $K_p = 1 \times 10^{-7}$. Thus, for P_{I_2} = 0.03 torr, P_I = 0.0015 torr, or 5% of P_{I_2}. At lower temperatures this percentage drops very rapidly. Under these conditions of negligible thermal dissociation and the absence of thermal transpiration effects, the pressure of I_2 is constant at 0.03 torr everywhere in the fluorescence cell. The concentration of I_2 molecules in the heated section of the cell is given by $[I_2]_H = P_{I_2}/k_B T_H$ where P_{I_2} = 0.03 torr and T_H is the temperature.

The observed first order decay constant is given by $k = k_{I_2}[I_2]_H$. By dividing k by $[I_2]_H$, k_{I_2} was determined over the temperature range T = 295° k to 643° k. The data are conveniently expressed in terms of the Arrhenius expression $k_Q = A_Q \exp(-E_Q/RT)$ where E_Q is the effective activation energy for quenching by species Q. A plot of $\ln k_{I_2}$ versus 1/T is shown in Fig. 7. The Arrhenius parameters are summarized in Table II. The activation energy is positive and k_{I_2} increases slightly with temperature. This is in disagreement with the

earlier study in which a large negative value for the activation energy was obtained. In view of the large error in the room temperature rate of the earlier study, it is quite possible that effects of incomplete mixing of I_2 vapor with the buffer gas perhaps further complicated by temperature gradients along the circulating system were responsible for the previously observed temperature effects. The activation energy determined in this study is + 0.5 kcal/mole indicating a relatively small energy barrier. At 643° K, k_{I_2} has increased to approximately 150% of its room temperature value.

$\underline{O_2}$

The deactivation of excited iodine atoms by oxygen molecules was found by Derwent and Thrush[29] to proceed predominantly by the near resonant E → E energy transfer process

$$I^*(5p^5\ ^2P_{1/2}) + O_2(^3\Sigma_g^-) \rightarrow I(5p^5\ ^2P_{3/2}) + O_2(^1\Delta g) \qquad (16)$$

which is endothermic by 0.8 kcal/mole. The room temperature rate constant of 2.6×10^{-11} cm^3 molecule^{-1} sec^{-1}[10] is extremely large. To study the temperature dependence of the O_2 quenching rate, the fluorescence cell coldfinger was immersed in a 0° C bath yielding a pressure of I_2 of 0.03 torr. O_2 was then admitted to the fluorescence cell, the pressure recorded, and the cell closed off while at room temperature. The main body of the fluorescence cell was then heated to a selected temperature and after equilibration, a run was taken to determine the fluorescence decay rate. The cell was then heated to

other temperatures and subsequent runs taken. This procedure was repeated several times at different temperatures. The cell was then cooled and evacuated and the procedure was repeated with a fresh fill of gas.

As described above, the iodine molecule concentration in the heated section was calculated by the relation $[I_2]_H = P_{I_2}/k_B T_H$ where $P_{I_2} = 0.03$ torr. In the case of a uniformly heated cell, the pressure of the added gas (in this case, 0_2) increases as the temperature is raised while the concentration remains constant (N_o). However, in the present case, because the coldfinger was not heated (11% of the total cell volume), as the temperature of the main body of the cell was raised the added gas concentration decreased slightly in the heated section and increased in the coldfinger. The concentration in the heated volume V_H at temperature T_H was related to the initial room temperature concentration N_0 by the relation

$$N_H = \frac{N_0(V_H + V_C)}{V_H + \frac{T_H}{T_C} V_C} \tag{17}$$

where V_C = coldfinger volume

T_C = coldfinger temperature.

This correction factor was employed for all of the data analyzed. The heated cell concentrations were always within 12% of the room temperature fill value even at the highest temperatures employed.

For each experimental run, the observed decay rate was given by $k = k_{I_2}[I_2]_H + k_{0_2}[0_2]_H$ for that particular temperature, T_H. Using

the best fit Arrhenius parameters for k_{I_2} found in the pure I_2 temperature dependence studies, the value of $k_{I_2}[I_2]_H$ was determined and subtracted from k. The value of k_{O_2} was then calculated, using Equation 17 to give the (corrected) value of $[O_2]_H$. The data are plotted in Fig. 8. The Arrhenius parameters are presented in Table II. The activation energy found was substantially greater than the value obtained by Deakin and Husain[11] and indicates a significant energy barrier for this process.

H_2, HD, D_2

The rate of quenching of I* at room temperature was found to differ significantly among these species, the quenching rate differing by more than two orders of magnitude for HD and D_2. It was of particular interest to study the temperature dependence of the quenching by these gases. The experimental procedure was identical to that followed for the O_2 temperature dependence studies. The experimental data and the best fit Arrhenius parameters are shown in Fig. 9-11 and Table II.

The quenching rate by H_2 increased dramatically to 5×10^{-13} cm^3 $molecule^{-1}$ sec^{-1} at 300° C. The activation energy of 2.6 kcal/mole is substantially higher than the value reported by Deakin and Husain.[11] The quenching rate by D_2 was found to decrease with temperature but much more slowly than reported in the earlier study. The temperature dependence of quenching by HD has not been previously reported. The rate was found to increase slightly with temperature to approximately double the room temperature rate at 300° C.

The temperature variation of the quenching of I* by H_2 and D_2 has been discussed in terms of resonant E → V + R transfer processes of the form[6]

$$I^* + H_2(v'',J'') \rightarrow I + H_2(v', J') + \Delta E_T \qquad (18)$$

where ΔE_T is the energy tranferred to translation. It was proposed that the rate of quenching of I* was dependent primarily on three factors. Channels for which ΔE_T was small should be greatly enhanced. Also the quenching rate should depend on the average collision frequency and on the population of the relevant v'', J'' states as a function of temperature. This elementary theory predicted a substantial positive activation energy for the quenching by H_2. The present results support this conclusion. For D_2, a small negative activation energy was predicted in quantitative disagreement with the earlier experimental results. The results of the present study do in fact show a very small negative activation energy for quenching by D_2. Further theoretical work on the H_2, HD, D_2 system would be beneficial. In particular, extension of earlier quantum mechanical studies to include temperature dependence would be of value.

References

1. D. Husain and R. J. Donovan, Adv. Photochem. 8, 1 (1971).
2. J. J. Deakin, D. Husain, and J. R. Wiesenfeld, Chem. Phys. Lett. 10, 146 (1971).
3. J. J. Deakin and D. Husain, J. C. S. Faraday II 68, 41 (1972).
4. I. H. Zimmerman and T. F. George, Chem. Phys. 7, 323 (1975).
5. I. H. Zimmerman and T. F. George, J. C. S. Faraday II 71, 2030 (1975).
6. R. J. Butcher, R. J. Donovan, and R. H. Strain, J. C. S. Faraday II 70, 1837 (1974).
7. D. H. Burde, R. A. McFarlane, and J. R. Wiesenfeld, Phys. Rev. A10, 1917 (1974).
8. D. H. Burde and R. A. McFarlane, Chem. Phys. 16, 295 (1976).
9. D. H. Burde, R. A. McFarlane, and J. R. Wiesenfeld, Chem. Phys. Lett. 32, 296 (1975).
10. D. H. Burde and R. A. McFarlane, J. Chem. Phys. 64, 1850 (1976).
11. J. J. Deakin and D. Husain, J. C. S. Faraday II 68, 1603 (1972).
12. D. H. Burde, Ph.D. Thesis, Cornell University (1976).
13. A. Yariv, Quantum Electronics, John Wiley and Sons, Inc., New York (1967).
14. I. Rubeska and B. Moldan, Atomic Absorption Spectrophotometry, ed. by P. T. Woods, Iliffe Books Ltd., London (1969).
15. R. J. Donovan, D. Husain, and L. J. Kirsch, Trans. Faraday Soc. 66, 2551 (1970).
16. C. C. Davis and R. A. McFarlane, J. Q. S. R. T. 18, 151 (1977).

17. I. Arnold, F. J. Comes, and S. Pionteck, Chem. Phys. 9, 237 (1975).

18. F. J. Comes and S. Pionteck, Chem. Phys. Lett. 42, 558 (1976).

19. D. E. O'Brien and J. R. Bowen, J. Appl. Phys. 40, 4767 (1969).

20. R. H. Garstang, J. Res. Natl. Bur. Std. US68A, 61 (1964).

21. I. Arnold, F. J. Comes, and S. Pionteck, Chem. Phys. 9, 237 (1975).

22. F. J. Wodarczyk, private communication.

23. P. L. Honston, private communication.

24. G. Starck and M. Bodenstein, Zeits. f. Elektrochemie 16, 961 (1910).

25. T. DeVries and W. H. Rodebush, J. Am. Chem. Soc. 49, 656 (1927).

26. G. M. Murphy, J. Chem. Phys. 4, 344 (1936).

27. M. L. Perlman and G. K. Rollefson, J. Chem. Phys. 9, 362 (1941).

28. JANAF Thermochemical Tables, Second Edition, Nat. Stand. Ref. Data Ser., Nat. Bur. Stand. (U.S.) 37 (1971).

29. R. G. Derwent and B. A. Thrush, Chem. Phys. Lett. 9, 591 (1971).

Table I

Second order quenching rate constants for the deactivation of $I^*(^2P_{1/2})$ at 295° K as determined by time-resolved atomic absorption.

Quenching Molecule	k_Q (cm^3 molecule^{-1} sec^{-1})		
	This work	Literature value	Ref.
I_2	$3.6 \pm 0.3 \times 10^{-11}$ (a)	3.0×10^{-11}	17
O_2	$2.5 \pm 0.3 \times 10^{-11}$ (b)	2.5×10^{-11}	11
H_2	$9.8 \pm 1.0 \times 10^{-14}$	1.1×10^{-13}	6
HD	$3.1 \pm 0.3 \times 10^{-13}$	3.2×10^{-13}	6
D_2	$2.4 \pm 0.3 \times 10^{-15}$	1.0×10^{-15}	3

(a) From Reference 9.

(b) From Reference 10.

Table II

Arrhenius Parameters ($k = A \exp(-E/RT)$) for the Deactivation of $I^*(^2P_{1/2})$

Quenching Molecule	$A(cm^3\ molecule^{-1}\ sec^{-1})$	E(kcal/mole)
I_2	$8.0 \pm 0.8 \times 10^{-11}$	0.5 ± 0.1
O_2	$1.6 \pm 0.5 \times 10^{-10}$	0.8 ± 0.2
H_2	$4.6 \pm 2.3 \times 10^{-12}$	2.6 ± 0.3
HD	$1.6 \pm 0.2 \times 10^{-12}$	0.9 ± 0.1
D_2	$2.3 \pm 0.8 \times 10^{-15}$	-0.2 ± 0.2

Figure Captions

Figure 1. Block diagram of the experimental apparatus used in the time-resolved atomic absorption studies.

Figure 2. Quenching of I* by H_2 at 295° K as determined by time-resolved atomic absorption.

Figure 3. Quenching of I* by HD at 295° K as determined by time-resolved atomic absorption.

Figure 4. Quenching of I* by D_2 at 295° K as determined by time-resolved atomic absorption.

Figure 5. Block diagram of the experimental apparatus used in the time-resolved atomic fluorescence studies.

Figure 6. Quenching of I* by I_2 at 295° K as determined by time-resolved atomic fluorescence.

Figure 7. Quenching of I* by I_2 as a function of temperature as determined by time-resolved atomic fluorescence.

Figure 8. Quenching of I* by O_2 as a function of temperature as determined by time-resolved atomic fluorescence.

Figure 9. Quenching of I* by H_2 as a function of temperature as determined by time-resolved atomic fluorescence.

Figure 10. Quenching of I* by HD as a function of temperature as determined by time-resolved atomic fluorescence.

Figure 11. Quenching of I* by D_2 as a function of temperature as determined by time-resolved atomic fluorescence.

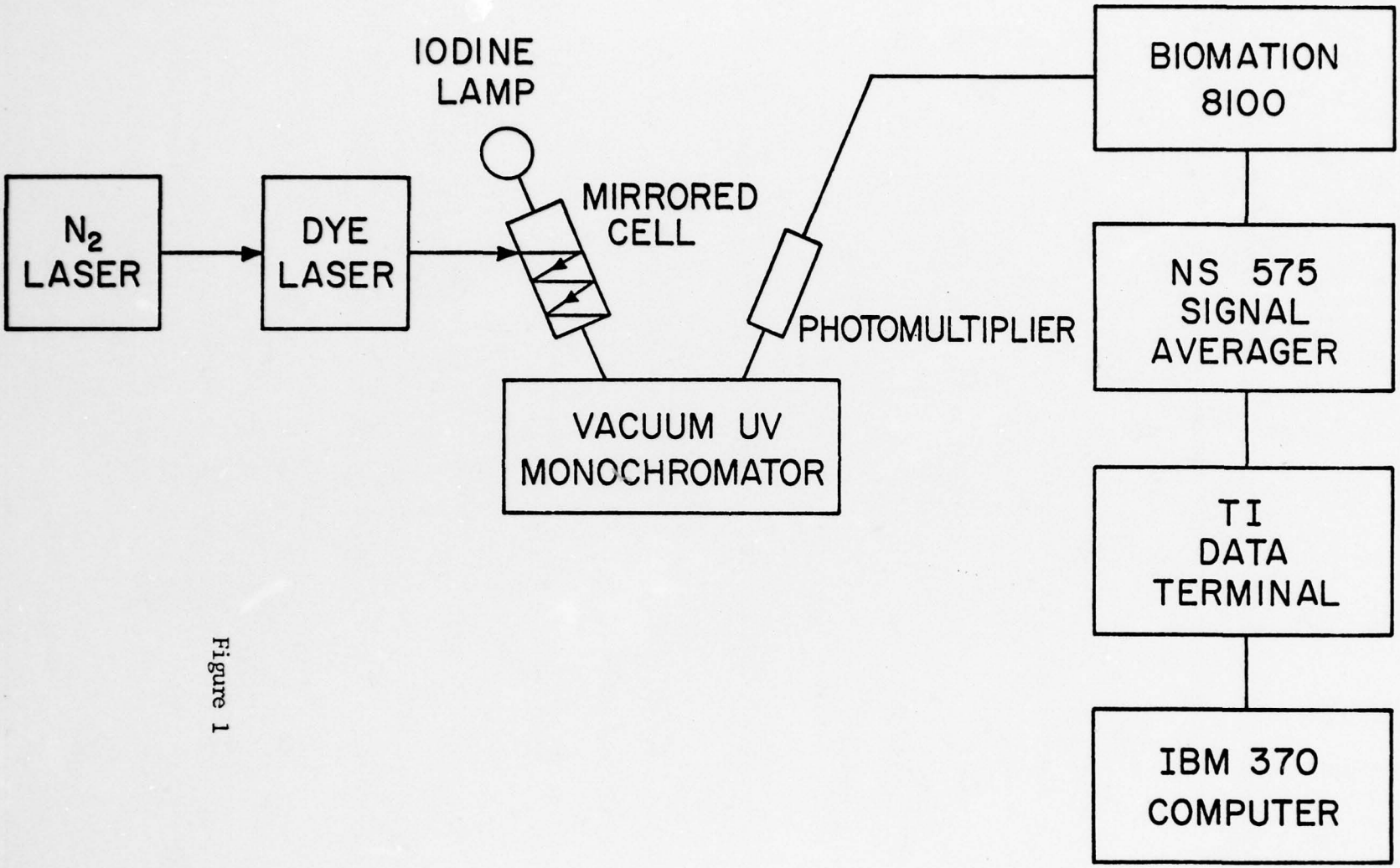
IODINE
LAMP
N_2
LASER
DYE
LASER
MIRRORED
CELL
PHOTOMULTIPLIER
VACUUM UV
MONOCHROMATOR
BIOMATION
8100
NS 575
SIGNAL
AVERAGER
TI
DATA
TERMINAL
IBM 370
COMPUTER

Figure 1

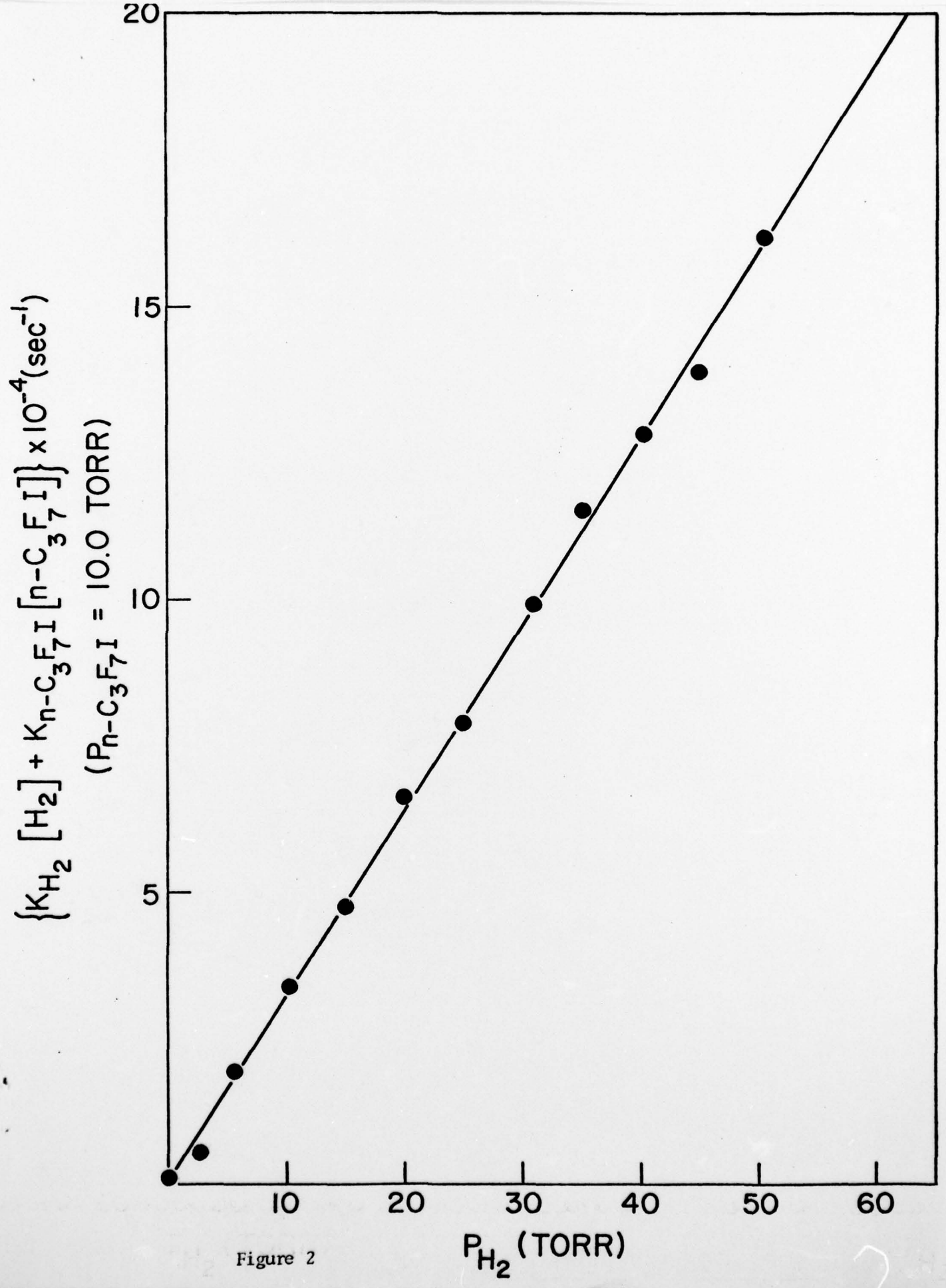
20
15
10
5
10
20
30
40
50
60
$\{K_{H_2}[H_2] + K_{n\text{-}C_3F_7I}[n\text{-}C_3F_7I]\} \times 10^{-4}(sec^{-1})$
$(P_{n\text{-}C_3F_7I} = 10.0\ TORR)$
P_{H_2} (TORR)

Figure 2

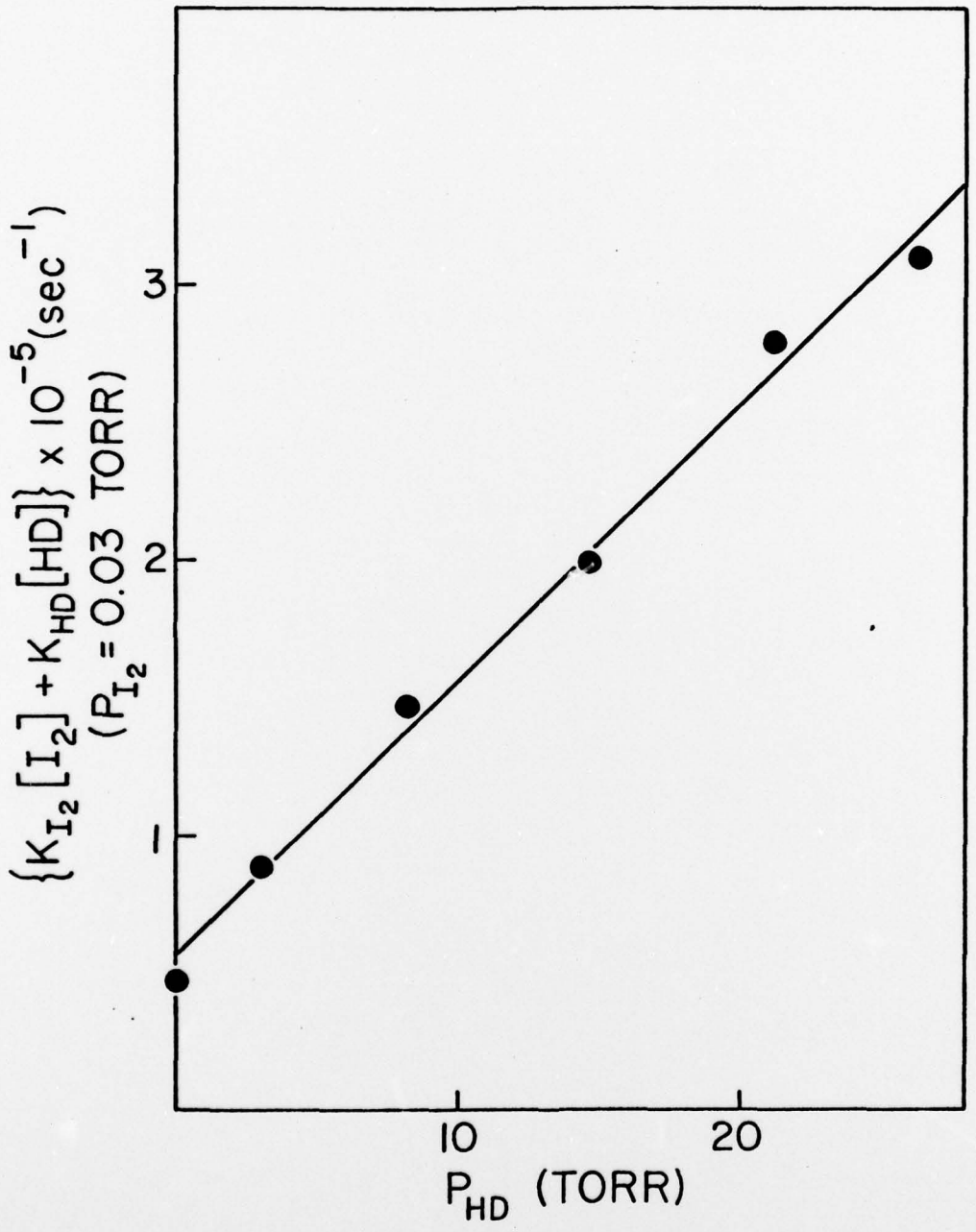

Figure 3

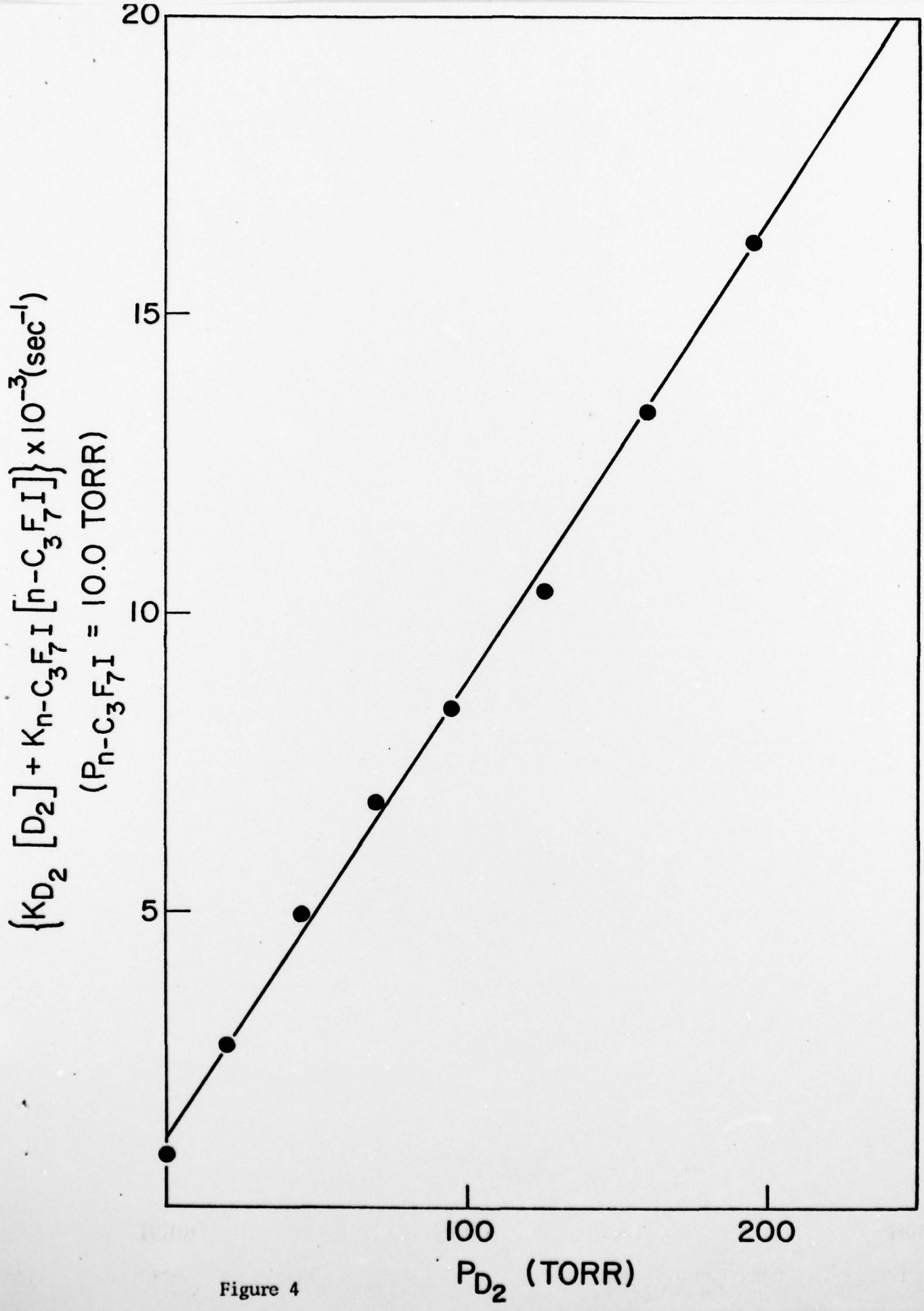
20
15
10
5
100
200
P_{D_2} (TORR)
$\{K_{D_2}[D_2] + K_{n\text{-}C_3F_7I}[n\text{-}C_3F_7I]\} \times 10^{-3}(sec^{-1})$
($P_{n\text{-}C_3F_7I}$ = 10.0 TORR)

Figure 4

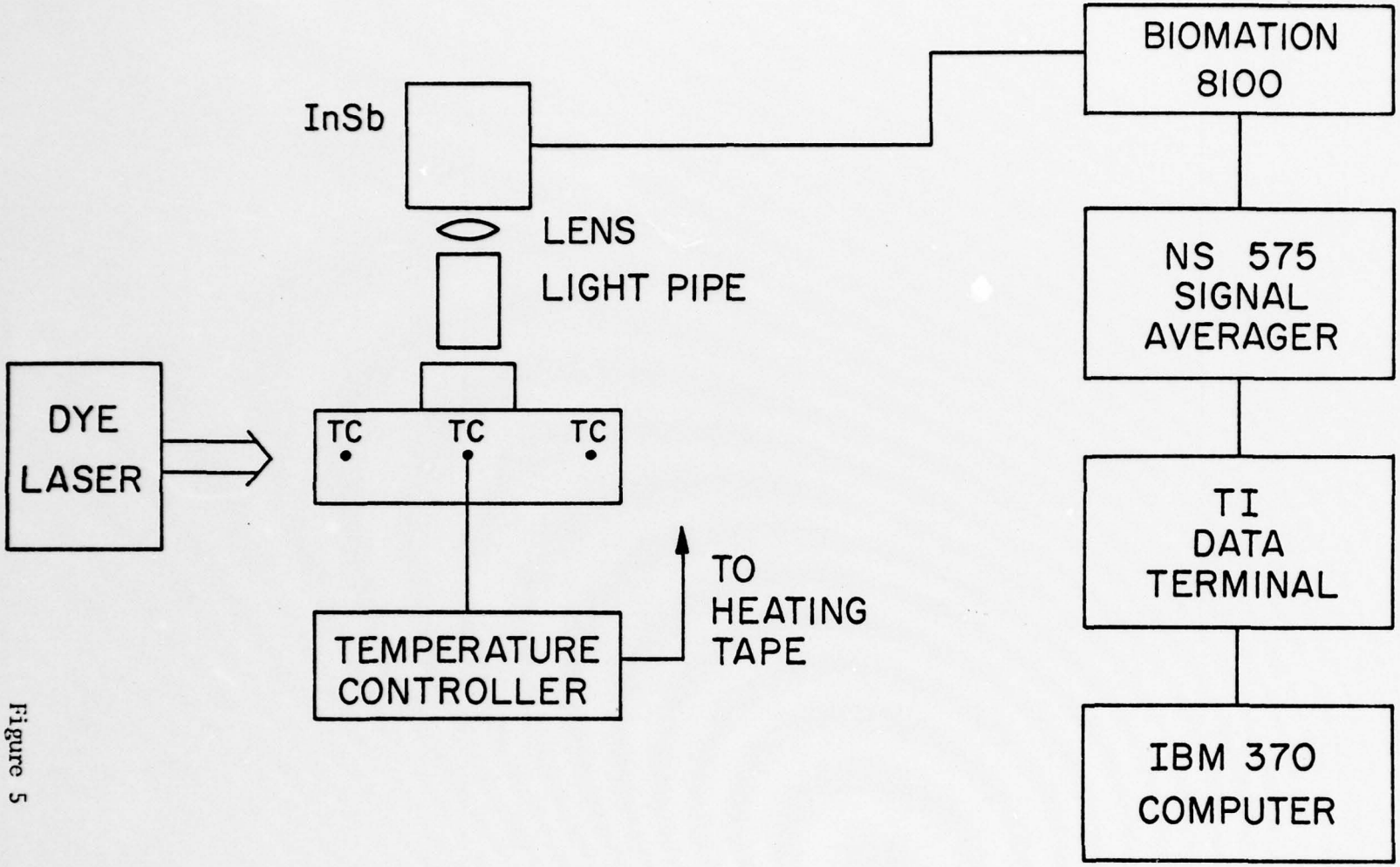
BIOMATION
8100
InSb
LENS
LIGHT PIPE
NS 575
SIGNAL
AVERAGER
DYE
LASER
TC
TC
TC
TI
DATA
TERMINAL
TO
HEATING
TAPE
TEMPERATURE
CONTROLLER
IBM 370
COMPUTER

Figure 5

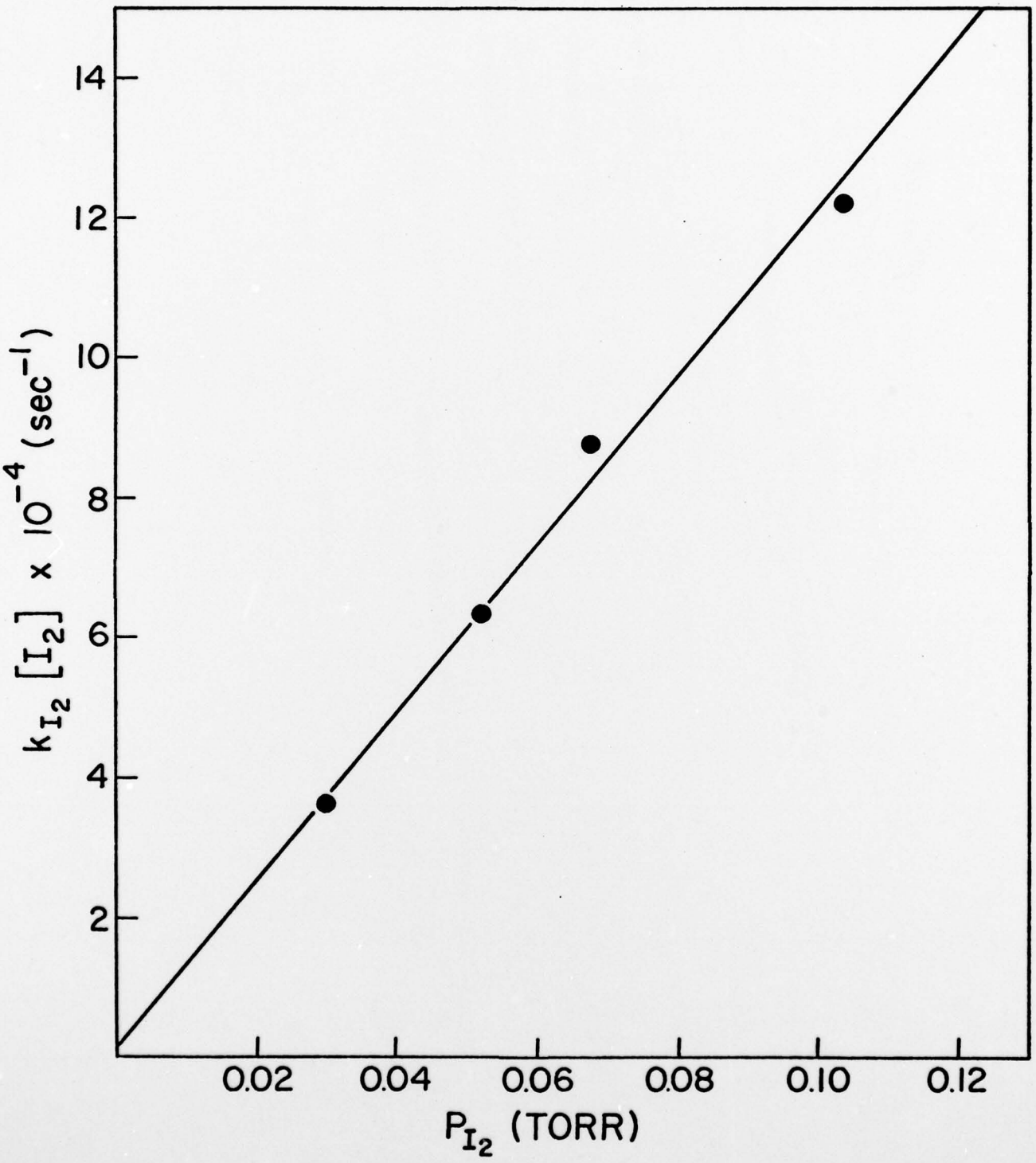
14
12
10
8
6
4
2
$k_{I_2}[I_2] \times 10^{-4}$ (sec^{-1})
0.02
0.04
0.06
0.08
0.10
0.12
P_{I_2} (TORR)

Figure 6

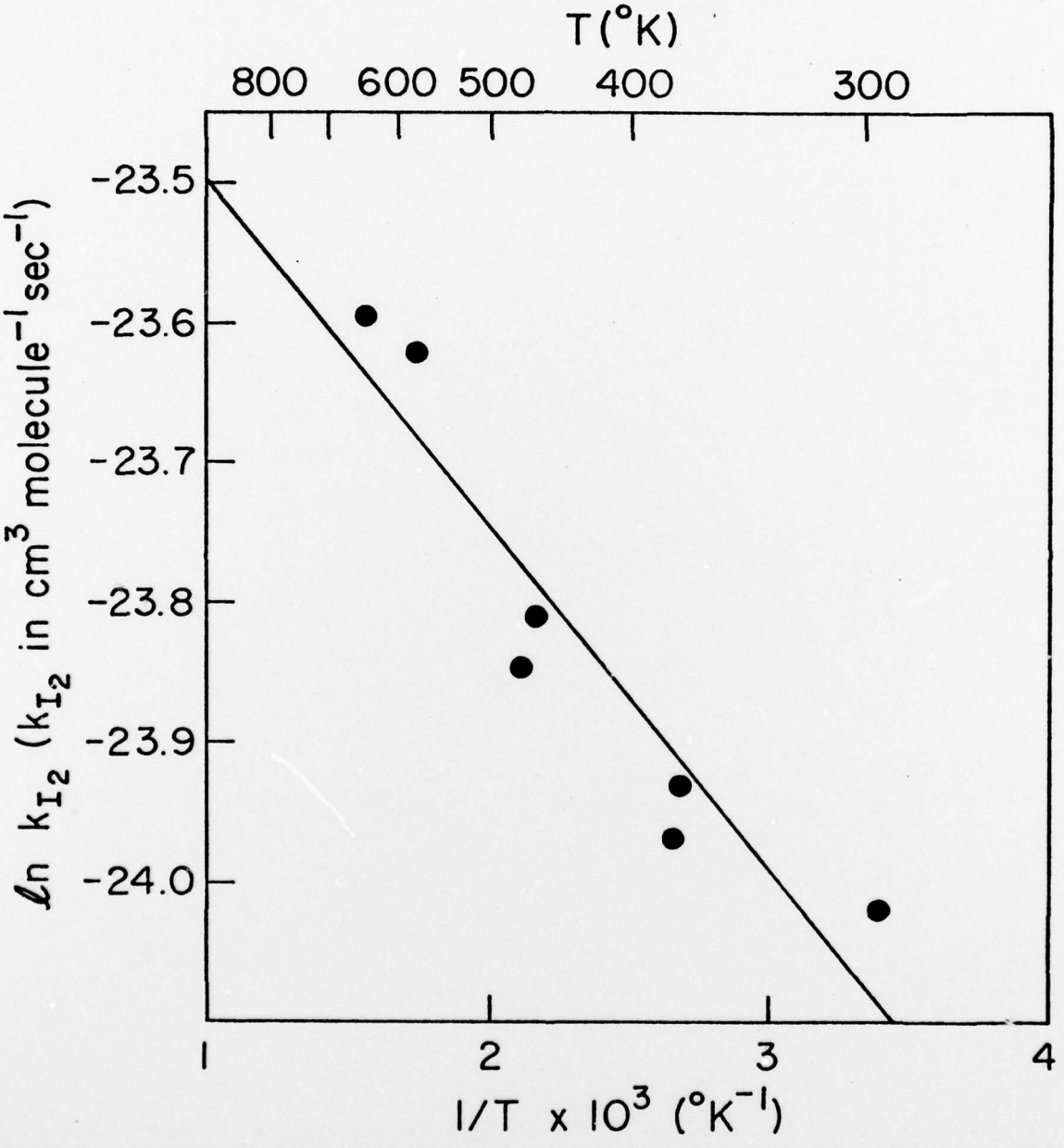
T(°K)
800
600
500
400
300
-23.5
-23.6
-23.7
-23.8
-23.9
-24.0
ℓn k_{I_2} (k_{I_2} in cm^3 $molecule^{-1}$ sec^{-1})
1
2
3
4
1/T x 10^3 ($°K^{-1}$)

Figure 7

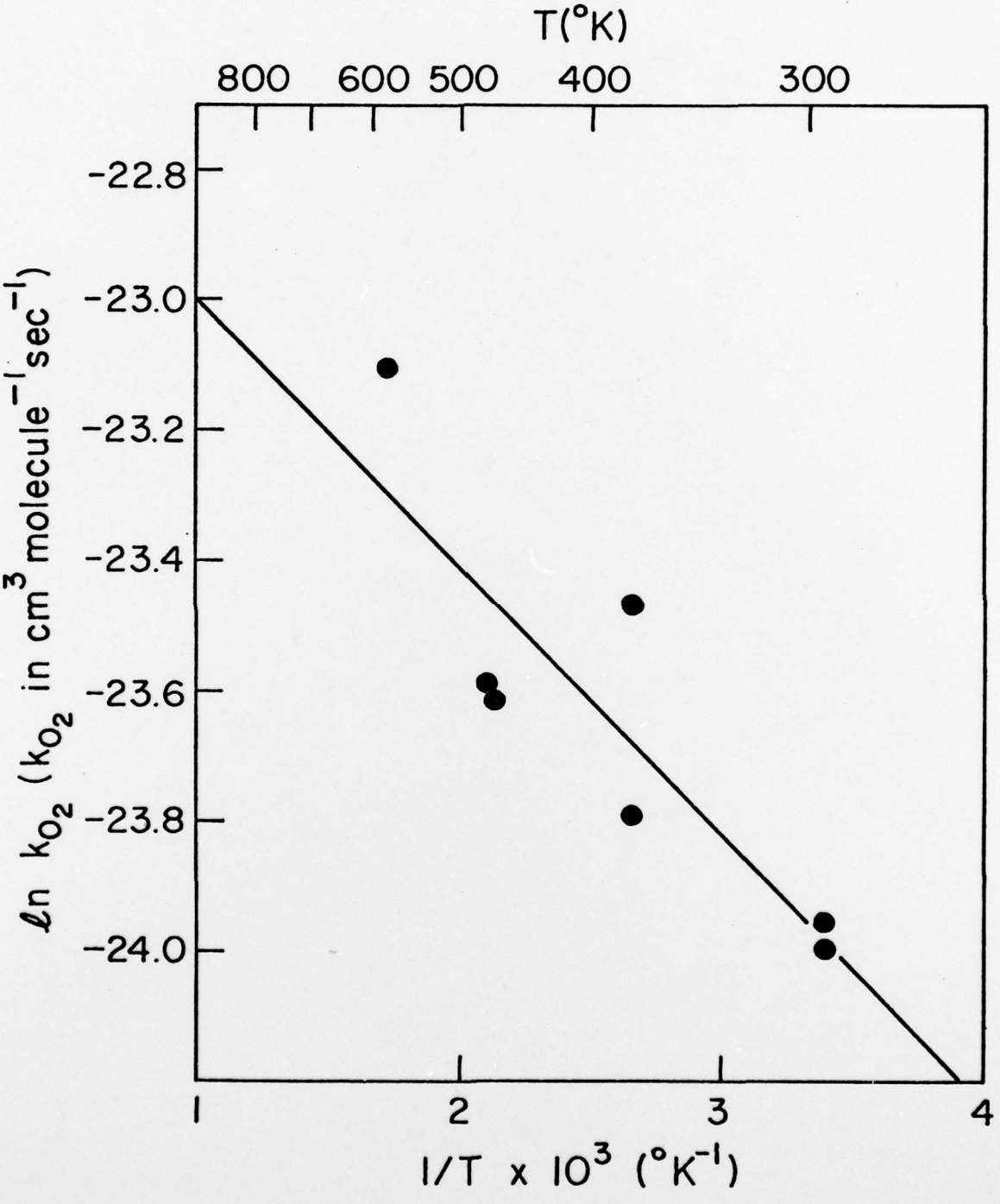
T(°K)
800
600
500
400
300
-22.8
-23.0
-23.2
-23.4
-23.6
-23.8
-24.0
ℓn k_{O_2} (k_{O_2} in cm^3 $molecule^{-1}$ sec^{-1})
1
2
3
4
1/T x 10^3 ($°K^{-1}$)

Figure 8

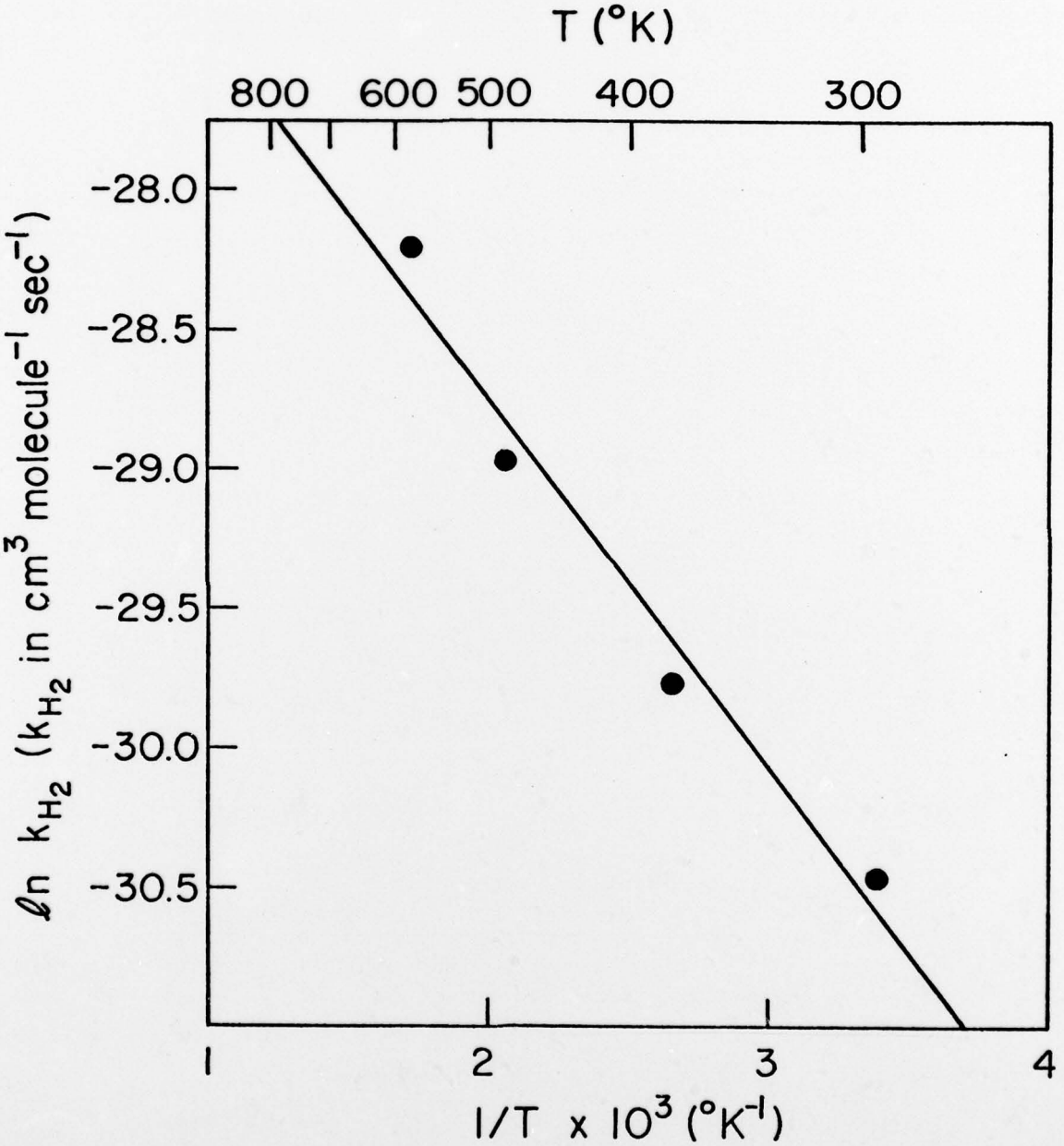
T (°K)
800
600
500
400
300
-28.0
-28.5
-29.0
-29.5
-30.0
-30.5
ℓn k_{H_2} (k_{H_2} in cm^3 $molecule^{-1}$ sec^{-1})
1
2
3
4
1/T x 10^3 ($°K^{-1}$)

Figure 9

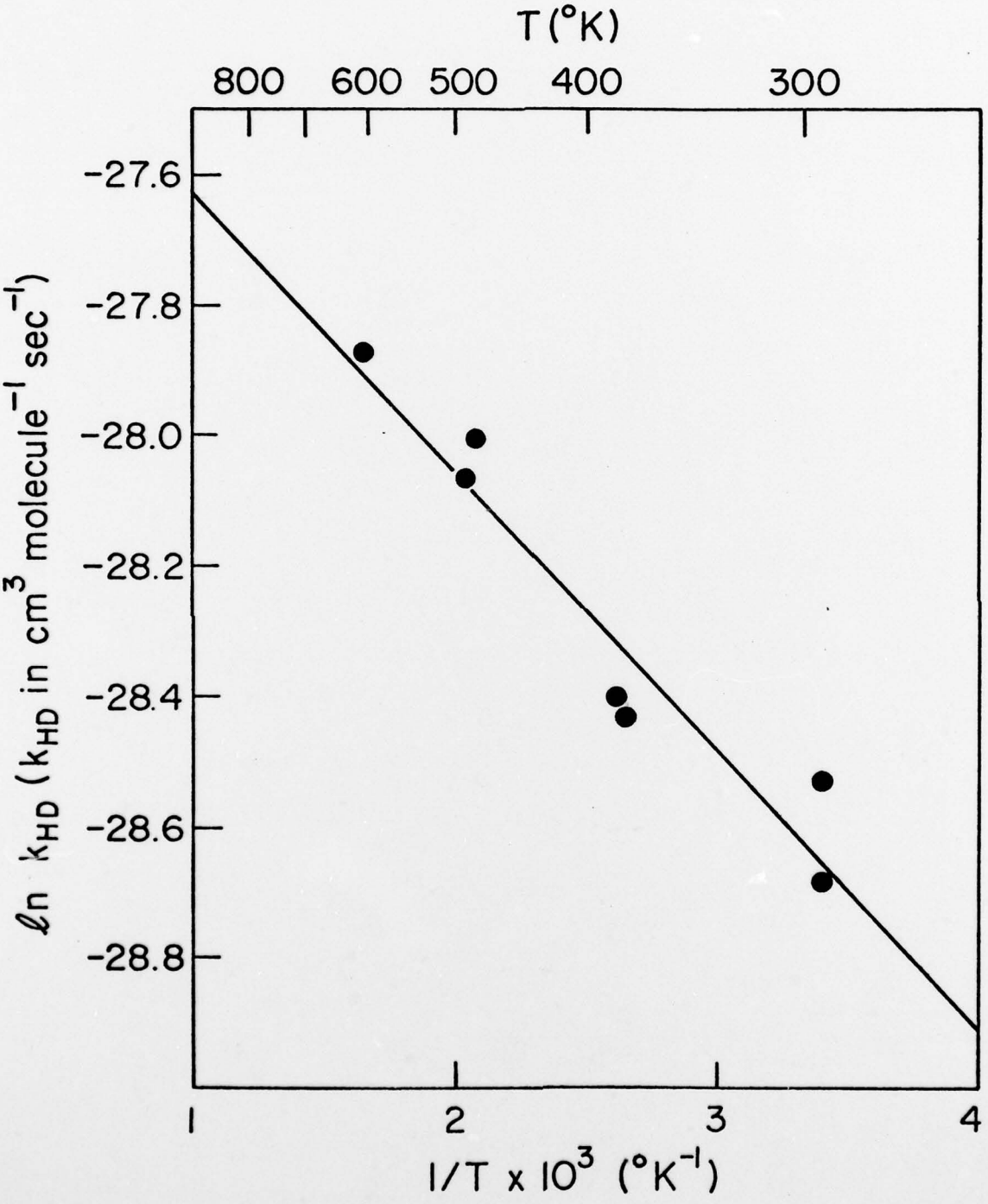
T(°K)
800
600
500
400
300
-27.6
-27.8
-28.0
-28.2
-28.4
-28.6
-28.8
ℓn k_{HD} (k_{HD} in cm^3 $molecule^{-1}$ sec^{-1})
1
2
3
4
1/T x 10^3 (°K^{-1})

Figure 10

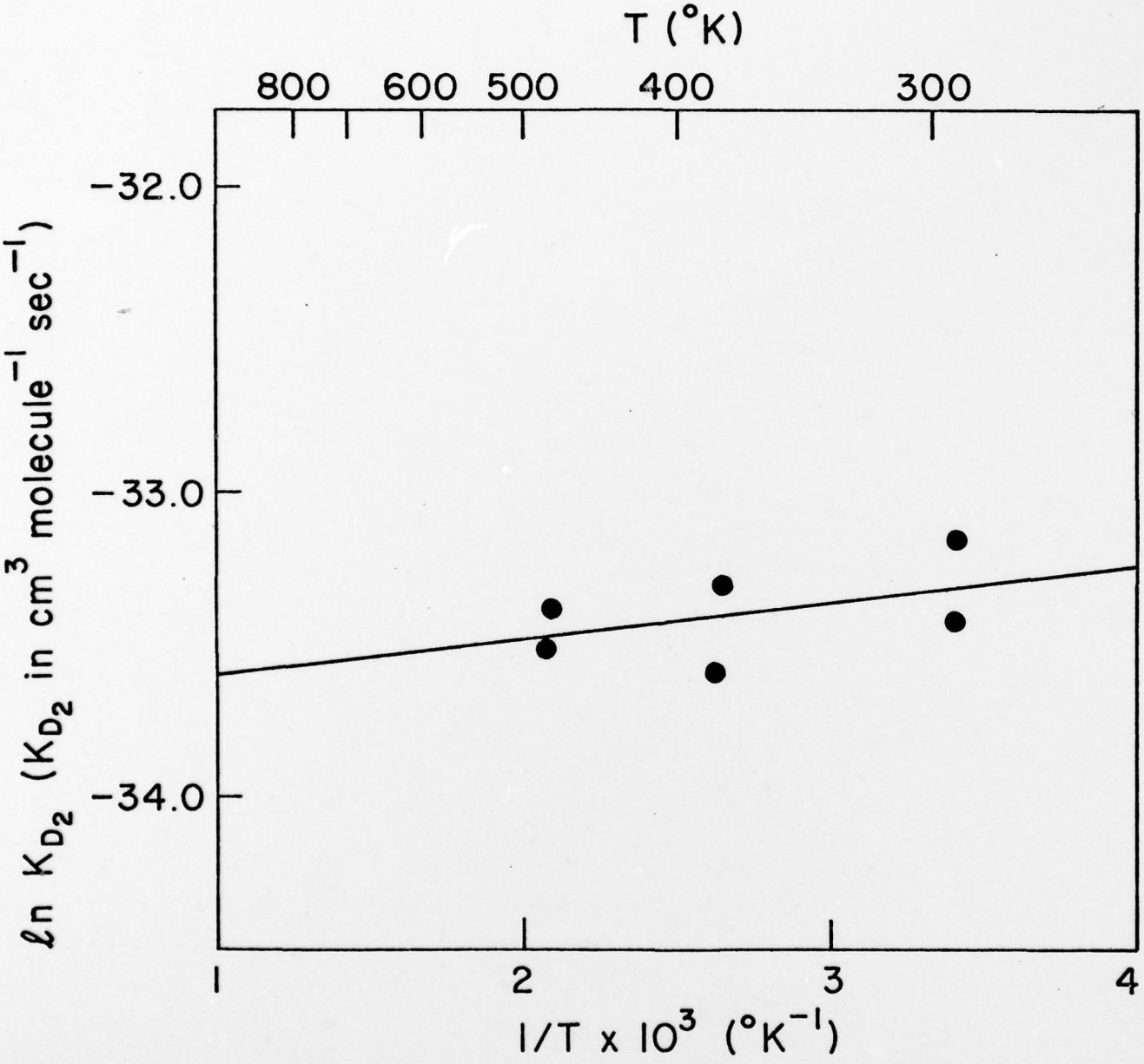
T (°K)
800
600
500
400
300
-32.0
-33.0
-34.0
ℓn K_{D_2} (K_{D_2} in cm^3 $molecule^{-1}$ sec^{-1})
1
2
3
4
1/T x 10^3 ($°K^{-1}$)

Figure 11